THE JOURNAL OF PHYSICAL CHEMISTRY C

pubs.acs.org/JPCC Article

Particle Size Distributions via Mechanism-Enabled Population Balance Modeling

Derek R. Handwerk, Patrick D. Shipman,* Christopher B. Whitehead, Saim Özkar, and Richard G. Finke*

Cite This: J. Phys. Chem. C 2020, 124, 4852−4880 Read Online

ACCESS | Metrics & More | Article Recommendations | Supporting Information

ABSTRACT: Mechanism-enabled population balance modeling (ME-PBM) was recently defined as the use of experimentally established (i.e., disproof-based, deliberately minimalistic, and pseudo-elementary step-based) mechanisms as more rigorous input for population balance models. ME-PBM addresses three long-sought goals: mechanism-based prediction and control of particle size distributions (PSDs), fitting PSDs by various mechanisms to test which mechanisms are refuted versus supported, and then also extracting rate constants for the most strongly supported mechanism from the wealth of kinetics information buried within the PSD. A full ordinary differential equation (ODE) approach is developed to the PBModeling that is a resurrection of Smoluchowski's 1918 approach, a little used, but powerful approach that in turn allows fitting of the information-laden PSD including its shape. The full details are reported of the 12 different particle-formation, pseudo-elementary step mechanisms tested in a disproof-based approach to the ME-PBM analysis of the PSDs and kinetics data for a prototype $Ir(0)_n$ nanoparticle-formation system. The ME-PBM analysis led to the discovery of a new particle formation mechanism that is a 1-step, but key, expansion of the classic Finke−Watzky two-step mechanism of nucleation, A → B, followed by autocatalytic surface growth, A + B → 2B. Specifically, the ME-PBM analysis yielded the new three-step particle-formation mechanism of A → B (rate constant k_1), A + B → C (rate constant k_2), and A + C → 1.5C (rate constant k_3), where A represents the monomeric nanoparticle precursor, B represents "small" nanoparticles, and C represents "larger" growing nanoparticles. A list of key conclusions is provided including the paradigm shifts for particle formation that (i) nucleation needs not be "instantaneous" or "burst" "to achieve narrow PSDs as postulated by the classical 1950s LaMer model; that (ii) instead nucleation can be and often is continuous, as first shown in 1997, yet still leads to narrow PSDs; and critically that (iii) narrow PSDs can and do result in spite of continuous nucleation because smaller particles grow faster than larger ones ($k_2 > k_3$), thereby allowing the smaller particles to catch up to the more slowly growing larger particles. Surface-ligand capping and other possible reasons that $k_2 > k_3$ are presented and discussed, as are additional conclusions, implications of the present studies, caveats, and needed additional studies. The goal of the present contribution is to follow up our first report of ME-PBM by providing the full details of our work to date so that others who wish to use ME-PBM in their own particle formations across nature, while fitting their own PSDs and testing their own mechanistic hypotheses, can readily do so.

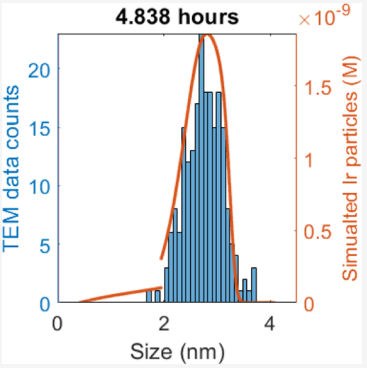

1. INTRODUCTION

Particle size and size distribution are key to the physical properties of catalyst and other particles or aggregates in nature.[1,2] Near-monodisperse (≤±15%)[3] if not narrower, approaching "monodisperse" particle size distributions (PSDs) are highly desirable. Because of this, mechanism-based, rational control of particle size and PSDs is a longstanding goal in nano- and other-particle science. However, the goal of reliable chemical mechanism-based particle size understanding and control has proved elusive to date.

Additionally, the mechanistic understanding of particle nucleation, growth, and agglomeration processes is at a critical crossroads. Classical nucleation theory (CNT) has been found to be inapplicable to many systems in nature that involve strong bonding.[4] Higher energy monomers lose their identity once they form even small nuclei in the system, such as the prototype $Ir(0)_n$ transition-metal nanoparticle formation system examined herein with its relatively strong Ir−Ir bonding,[4] rendering CNT inapplicable to such strong-bonding systems (see the list of references supporting this statement summarized elsewhere[4]). Moreover, the one historically highly cited model of particle formation that uses CNT as its basis, the words-only 1950 LaMer model of putative "instantaneous" or "burst" nucleation followed by "diffusion-controlled growth", has now been compellingly disproved by a critical analysis of 1953 papers in the literature that cite the LaMer model.[5] The disproof of the

Received: December 3, 2019
Revised: January 12, 2020
Published: February 14, 2020

classic LaMer model is of more than passing interest given that 1762 (i.e., 90%) of 1953 citations of the LaMer model (as of March 2019) simply cite the LaMer model as if it were accepted fact—often citing the mathematical assumption of "instantaneous nucleation" as if it had exceptional experimental support.[5] It has no compelling support.[5] The 69 year allure of the LaMer model to putatively explain "monodisperse" particle formation at least previously is clear: putative "burst" nucleation, followed by growth, was previously the only postulated ("known") way that very narrow, "monodisperse" particles could *in principle* have been formed—the word "monodisperse" appearing in the titles of nine of LaMer's early papers.[5]

However, as pointed out elsewhere, the LaMer model is actually a growth model that says nothing about nucleation.[5] Rather, the LaMer hypothesis bypasses the challenging topic of nucleation by assuming that nucleation is "instantaneous", a mathematically necessary assumption at the time to allow tractable math of that creative growth model. However, then one asks, "how else besides putative 'burst nucleation' can one attain narrow PSDs by self-assembly syntheses that often involve ≥tens of thousands of discrete chemical steps?". The present work bears directly on this critical question, in the field of particle formations across nature, of how near-monodisperse PSDs can ever form from a self-assembly reaction, especially if continuous nucleation[6] is present, an inherently PSD-broadening process.

In a recent paper we have provided the initial answers to the above questions by performing mechanism-enabled population balance modeling (ME-PBM) in a disproof-based manner that considers 12 possible particle-formation pseudo-elementary step mechanisms.[7] That ME-PBM in turn, led to three paradigm shifts in the understanding of particle formation, specifically (i) that nucleation is often continuous as first discovered in 1997;[6] (ii) that autocatalytic growth of smaller particles is, at least in the case of transition metal, $Ir(0)_n$ nanoparticles, faster than that of larger particles. This allows the smaller particles to "catch up" in size with the slower growing larger ones, thereby achieving otherwise surprisingly narrow PSDs from self-assembly syntheses involving continuous nucleation and subsequent parallel growth; and hence (iii) that nucleation needs not be "instantaneous" or "burst" in order to achieve relatively narrow PSDs. However, the necessary full details of the ME-PBM that led to these conclusions, critical details so that others can employ ME-PBM in their own work and particle-formation problems, have not been reported until this paper.

The goal of the present paper is to report those needed full details so that others can reproduce, refine, and otherwise build off our initial ME-PBM work. Included below to start are required background sections that cover the following: classical PBM; the concept of ME-PBM; the needed, experimentally determined, minimalistic nanoparticle formation mechanisms; the critical, required molecular mechanism of nucleation; classical approaches to solving the PBM equation; and the full ODE approach to the PBM in the present work in which we resurrect Smoluchowski's classic 1918 approach. There is some deliberate overlap with our first paper[7] (as referenced in what follows), but only that necessary to attain our goal of fully enabling others with ME-PBM, including readers previously unfamiliar with any type of population balance modeling.

1.1. Classical Population-Balance Modeling. The concept of population balance modeling (PBM)[8−13] is conceptually straightforward: PBM can be used to describe any system of countable entities[8] where "a distribution of properties changes in time and perhaps also in space".[10] A simple, word statement of a population balance (PB) is given in eq 1 illustrated for an individual particle of a given size, j, but where the PB model is across all particles (all values of j)

$$(\text{Input})_j - (\text{output})_j = (\text{accumulation})_j \tag{1}$$

That is, for every particle in the dynamic particle distribution ("population") one is simply keeping track of the evolving particle population using the law of mass balance on each and every particle size to, thereby, determine the PSD as a function of time, including the key final PSD. "All" that one then needs in practice for PBM in the ideal case is the following: (i) the actual particle formation mechanism(s); which then and in turn yield (ii) the system of ordinary differential equations (ODEs) corresponding to those mechanistic steps as input into the PBM; (iii) the starting/boundary conditions for the system at hand, and (iv) the ability to integrate (numerically) the systems of ODEs to see what average particle size and PSD results. However, the Achilles heel of PBM historically has been the lack of the required input mechanisms and, hence, the lack of the corresponding, correct, associated ODEs to describe the dynamics of the system at hand. Especially critical, we will see, is to have the experimentally determined nucleation mechanism, as those key initial steps are what starts out the particle formation process and, hence, are required input for reliable PBModeling.

As conceptually straightforward as PBM is, the mathematics and implementation of classical PBM are much less straightforward if not complex. Consider the case of larger, approaching even 0.1 μm-sized particles that, then, consist of the assembly of tens of millions of monomers. In such cases, keeping track of the accumulation eq 1 for each value of j yields a system of tens of millions of ODEs. Hence, in classical PBM one derives a partial differential population balance equation (PBE) for a function of continuous particle size (and time). With a number of assumptions, one can then generate the general PBE. Key assumptions underlying classical PBM are

1. That one has a sufficient number of particles to approximate a continuum of particle sizes;
2. That each particle behaves identically and has an identical trajectory in particle phase space, the population balance starting from a single particle and assuming that all other particles behave identically (e.g., along a particle-length or volume axis, or, if the particle shape is known, equivalently along a particle-size axis);
3. That, typically, only a single internal coordinate (i.e., volume, length, or size) is important for the particle formation process. Relevant derivations related to eq 2 are provided in the Supporting Information. Multidimensional PBM as well as stochastic PBM are current topics in the PBM literature available to the interested reader.[11]

For volume, V, as the particle property (i.e., internal coordinate) of interest, the general PBE is[8]

$$\frac{\partial n(V,t)}{\partial t} + \frac{\partial}{\partial V}[G(V,t)n(V,t)] = B(V,t) - D(V,t) \tag{2}$$

where $n(V,t)$ is the number of particles in the volume (i.e., size) increment from V to $V + dV$ at time t, and $G(V,t)$, $B(V,t)$, and $D(V,t)$ are, respectively, the crucial growth rate (with dimensions volume/time) and birth and death functions (with dimensions number/time) for the particles in that volume increment dV at time t.

https://dx.doi.org/10.1021/acs.jpcc.9b11239
J. Phys. Chem. C 2020, 124, 4852−4880

A careful reading of the PBM literature reveals the largely ignored Achilles heel of PBM, namely, the "choice" of the birth (i.e., the crucial nucleation), growth functions (e.g., chemical-reaction controlled vs LaMer-type[5] diffusion-controlled), and death (e.g., ligand capping, agglomeration, and so on) functions required as input into any (reliable) PBM. That is, the Achilles heel of PBM has been the lack of knowledge of the mechanism(s) of particle formation; the lack of what we recently defined as reliable, minimum-mechanism-enabled-PBM.[7]

Highly relevant here is a 2013 PBM paper[14] noting that "the assumption that nuclei emerge at a single size is made in the vast majority of all publications that use PBE models and take nucleation into account"[14,15]—or really attempt to take nucleation into account. This assumption is basically the now disproved assumption[5] of physically impossible[5] "instantaneous nucleation"[5] that arose by postulate in LaMer's model out of mathematical convenience.[5] This "instantaneous nucleation" assumption is just the assumption and use of the LaMer model[5] and its underling CNT. The wide prior citation of the now disproven[5] "instantaneous or burst nucleation" postulate of the LaMer model is clear: previously there was no other, experimentally documented and PBModeled way to form near-monodisperse PSDs.

Noteworthy here is that in his classic 1964 text on population balance, pioneer Randolph notes (on p. 11)[8] the critical importance of having correct, experimentally determined "birth and death terms", because "a priori progress and predictions of particle-size distributions... will be hindered" (to say the least) until those needed birth (B) and death (D) terms in eq 2 become available. Another leading expert on PBM, Ramkrishna,[11] similarly notes as the final summary point in his extensive review on "The Status of Population Balances",[11] that "considerable... additional effort is required in identifying 'frequency functions'... directly from experimental data." In chemical terms, the needed "frequency functions" are the experimentally determined, rigorous, disproof-based, Ockham's-razor-obeying, balanced reaction-formulated, chemical reaction mechanisms. In short, the missing part and Achilles' heel of PBM until now have been the lack of the required, minimalistic, disproof-based particle-formation mechanisms for especially nucleation, but also growth, ligand capping, and agglomeration (and, probably, other steps eventually such as particle fragmentation), experimentally demonstrated mechanistic pseudo-elementary steps that can then be combined with PBM to permit what we define as mechanism-enabled PBM.[7] The above quotes from multiple different leaders in classic PBM in turn strongly support our thesis that mechanism-enabled PBM has not been defined nor existed until now.[7]

1.2. Concept of ME-PBM. The concept of ME-PBM is straightforward and is defined below in more detail than given recently:[7] in ME-PBM one starts from rigorously obtained, deliberately minimalistic, extensively disproof-based[16,17] and therefore reliable mechanisms of particle formation and agglomeration.[4,6,18−26] One then uses those (as-reliable-as-presently-available) minimum mechanisms to underpin and thereby enable PBM of nano and larger particle formation and agglomeration.[6,24,27−39] ME-PBM is, then, the simplest solution to the 55 year-old problem that has existed since the 1964 introduction[8,9] of PBM, namely, the need to provide experimentally based birth ($B(V,t)$), growth ($G(V,t)$), and death ($D(V,t)$) functions for the generalized PBM eq 2. Mechanism-enabled PBM is of significant interest as an in-principle powerful way to understand, and thereby potentially manipulate and control from the start, particle size- and size-distributions—that, in turn, are generally critical to controlling the properties and hence applications of those particles.

As straightforward as the concept of ME-PBM is, ME-PBM was not possible until now because of four reasons (four previously missing advances): (i) CNT had not been compellingly disproved for strong-bonding systems, so that it was not previously generally appreciated that CNT cannot be used in PBM of at least strong-bonding systems;[4,6,23,24] and (ii) the overwhelming evidence disfavoring[5] the 1950 LaMer growth model and its assumed "instantaneous" ("burst") nucleation had not been critically reviewed,[5] so that it was not better known until 2019[5] that the LaMer model with its assumption of "burst nucleation" cannot be used to enable reliable PBM—in fact if used will disable the PBM. The importance of knowing the correct, experimental nucleation mechanism in order to start the PBM out correctly is a critical insight—especially in light of the fact quoted above of "The assumption that nuclei emerge at a single size is made in the vast majority of all publications that use PBE models and take nucleation into account".[14,15] Put another way: the vast majority of all publications that use PBE models while trying to take nucleation into account cannot be correct; they are incorrect/disabled from their very start. Hence, the third reason ME-PBM was not possible until now is that (iii) the crucial molecular mechanism of nucleation for a prototype system that could be used in ME-PBM of at least a metal nanoparticle did not exist until 2017.[23] Finally, (iv) it was not widely appreciated that the needed minimum mechanisms for the growth and agglomeration steps do now exist, as shown in Scheme 3 that follows, so that it was not widely appreciated previously that deliberately minimalistic mechanisms do exist at least in pseudo-elementary step form (vide infra, Scheme 3) and can be used along with an experimentally known nucleation mechanism to properly mechanistically enable at least one's initial ME-PBMs.

1.3. Prototype Ir(0)$_n$ Nanoparticle Formation System Examined—Including the Required Molecular Mechanism of Nucleation. Scheme 1 below, reproduced from our recent publication,[7] shows the prototype Ir(0)$_n$ formation system examined herein. The system begins from the well-characterized and atomically precise[40,41] precursor and precatalyst $\{(1,5\text{-COD})Ir^{I}\cdot POM\}^{8-}$ (POM = the polyoxometalate, $P_2W_{15}Nb_3O_{62}^{9-}$). The Ir(0)$_{\sim 730}$ nanoparticles were prepared from the $\{(1,5\text{-COD})Ir^{I}\cdot POM\}^{8-}$ precursor/precatalyst as in previous works.[6,40,41] Reduction of this precursor under H_2 yields average-size Ir(0)$_{\sim 730}$ nanoparticles under the specific conditions employed herein and the PSDs versus time that will be shown and quantitatively analyzed later in the paper.

1.4. Required, Critical Molecular Mechanism of Nucleation. Only recently was the final, critical, previously missing mechanistic piece needed to finally be able to introduce rigorous ME-PBM, namely, a molecular mechanism of nucleation for the system at hand. In the present case of prototype Ir(0)$_n$ nanoparticle formation, Scheme 2,[23] that rare,

Scheme 1. Experimentally Determined, Balanced Reaction Stoichiometry for the Formation of Ir(0)$_{\sim 730}$ Nanoparticles; Adapted from ref 7 with Permission

$$730\ [(1,5\text{-COD})Ir{\cdot}P_2W_{15}Nb_3O_{62}]^{8-} + 1825\ H_2 \longrightarrow$$
$$Ir(0)_{\sim 730} + 730\ \text{cyclooctane} + 730\ H^+ + 730\ [P_2W_{15}Nb_3O_{62}]^{9-}$$

https://dx.doi.org/10.1021/acs.jpcc.9b11239
J. Phys. Chem. C 2020, 124, 4852−4880

Scheme 2. (Part A) Molecular-Level, Alternative-Termolecular Mechanism of Nucleation of $Ir(0)_n$ Nanoparticle Formation; (Part B) The Same Alternative-Termolecular Mechanism in Terms of "A·L" Nomenclature; Reprinted with Permission from the Supporting Information of ref 7; Copyright 2019 American Chemical Society

Part A:

$$2\ (COD)Ir{\bullet}POM^{8-} + 4\ solv \underset{}{\overset{K_{Diss}}{\rightleftharpoons}} 2\ (COD)Ir(solv)_2^{+} + 2\ POM^{9-}$$

$$2\ (COD)Ir(solv)_2^{+} + (COD)Ir{\bullet}POM^{8-} + 7.5\ H_2 \xrightarrow{k_{1(alt.termol)}} 3Ir(0) = Ir(0)_3 + POM^{9-} + 3H^{+} + 3\ cyclooctane + 4\ solv$$

$$\text{Net:}\quad 3\ (COD)Ir{\bullet}POM^{8-} + 7.5\ H_2 \longrightarrow 3\ Ir(0) = Ir(0)_3 + 3\ POM^{9-} + 3H^{+} + 3\ cyclooctane$$

Part B:

$$2\{A{\bullet}L + 2\ solv \rightleftharpoons A(solv)_2 + L\}$$

$$2\ A(solv)_2 + A{\bullet}L \longrightarrow 3B(= B_3) + L + 4\ solv$$

$$\text{Net:}\quad 3\ A{\bullet}L \longrightarrow 3B(= B_3) + 3\ L$$

experimentally determined molecular mechanism of nucleation is termed the "alternative-termolecular" mechanism of nucleation ("alternative termolecular" to distinguish it from the simpler, experimentally disproved[23] mechanism of nucleation that might have been net termolecular in the precursor $\{(1,5\text{-}COD)Ir^{I}{\cdot}POM\}^{8-}$, POM = the polyoxometalate, $P_2W_{15}Nb_3O_{62}^{9-}$).

Part A of Scheme 2 shows the molecular-level alternative-termolecular nucleation mechanism of $Ir(0)_n$ nanoparticle formation from the molecular, well-characterized $\{(1,5\text{-}COD)\text{-}Ir^{I}{\cdot}POM\}^{8-}$ precursor. Different nucleation mechanisms of (i) bimolecular in Ir (i.e., Ir_2), (ii) simple termolecular in Ir (Ir_3), and (iii) importantly all higher molecularity, $n > 3$, Ir_n, nucleation mechanisms were specifically considered, and disproved, in a 2017 publication.[23] However and as a further test of the nucleation mechanism in the present $Ir(0)_n$ nanoparticle formation system, third- (Ir_3) as well as fourth-order (Ir_4) nucleation mechanisms will be tested as part of the ME-PBM studies which follow. Part B of Scheme 2 illustrates the alternative-termolecular nucleation mechanism in terms of the "A·L" (L = ligand) nomenclature that will be used to implement it in the ME-PBM that follows where A·L specifically is $A{\cdot}L = \{Ir^{I}(1,5\text{-}COD)^{+}{\cdot}POM^{9-}\}^{8-}$.

Such experimentally determined, molecular-level mechanisms of nucleation are a rarely achieved but critical goal for each and every one of the myriad of phase-change processes across nature that involve nucleation.[42−51] Noteworthy here is the paradigm shift away from CNT that typically has been used (in inappropriate, incorrect, and ultimately futile attempts) to try to underpin PBMs of particle formation in at least high-energy, low solubility, monomer systems that exhibit strong monomer−monomer bonding[4,5,23,24] where the identity of the monomer is lost in the nucleus as is the case for Ir_3. The paradigm shift is, instead, toward low molecularity, $n = 2{-}3$, $(monomer)_n$ nucleation[4,5,23,24] for such strong-bonded systems where the "monomer" loses its prior chemical identity in a small kinetically effective nucleus[4] such as Ir_3 as in the $Ir(0)$ nanoparticle system treated herein[23] [i.e., and as opposed to weak-bonding systems such as alkane (RH) aggregates in the gas phase, where the alkane retains its molecular chemical identity in the $(RH)_n$ nucleus and where CNT does work].[46,50] In short, the important point for the present contribution is that unless one knows the true, molecular mechanism of nucleation, one cannot possibly start off the "population" and resultant "balance" in the PBModel correctly, except conceivably by accident. In the absence of an experimentally known nucleation mechanism, one can expect erroneous conclusions to result regarding the particle formation process even in the hands of PBM experts, as occurred from a 2014 PBM study.[52]

1.5. Needed, Experimentally Determined, Minimalistic Nanoparticle Formation Mechanisms. The required experimentally based, minimalistic nanoparticle-formation mechanisms with which to enable the ME-PBM in terms of pseudo-elementary steps[6,53] (i.e., that are sums of true elementary steps[6,53]) have been developed deliberately and painstakingly over the past 20+ years,[6,18−26] primarily (albeit not exclusively[19−21]) for the prototype $Ir(0)_n$ nanoparticle formation system. Now available for use with the PBM approach are pseudo-elementary-step based, minimalistic nanoparticle formation mechanisms consisting of two-step,[6] three-step,[18] and two four-step[19−22] mechanisms. Those kinetic models contain the pseudo-elementary steps in Scheme 3 of (i) now classic slow, continuous nucleation[6] as well as autocatalytic surface growth,[6] (ii) two types of agglomeration (bimolecular and autocatalytic agglomeration[18−21]), and (iii) secondary autocatalytic surface growth.[22] In addition recently and quite importantly, compelling evidence has appeared for a ligated precursor[23,54] and ligated-particle product[54] reversible (equilibria) steps that promise to be crucial in accounting for ligand-based particle size and size distribution control.[55] These last, ligand-dependent steps, not shown in Scheme 3, are the aforementioned (iv) ligated precursor $A{\cdot}L \rightleftharpoons A + L$,[23,54] and (v) ligated-particle product $B{\cdot}L \rightleftharpoons B + L$,[54] pseudo-elementary steps.

Important to note here—but still not well-recognized—is that pseudo-elementary steps obtained through disproof-based scientific experiments are often the best one can do initially for complex, multistep reactions such as nanoparticle formation. Pseudo-elementary steps for more complex reactions are therefore a kinetic and mechanism necessity—the initial building blocks—in formulating the more detailed mechanisms for such more complex chemical reactions, as Noyes' classic work on oscillating reactions employing pseudo-elementary steps teaches.[53] Furthermore, the correct pseudo-elementary steps are composites of the true, underlying elementary steps.[53,56] In favorable cases,[56] those underlying elementary steps can then be uncovered—via the initial pseudo-elementary step approach—and shown to add up to the curve-fit pseudo-elementary steps, as in a pedagogically valuable example

https://dx.doi.org/10.1021/acs.jpcc.9b11239
J. Phys. Chem. C 2020, 124, 4852−4880

Scheme 3. Deliberately Minimalistic, Ockham's Razor-Obeying Mechanistic Steps for Transition-Metal Nanoparticle Formation; Adapted from ref 7 with Permission

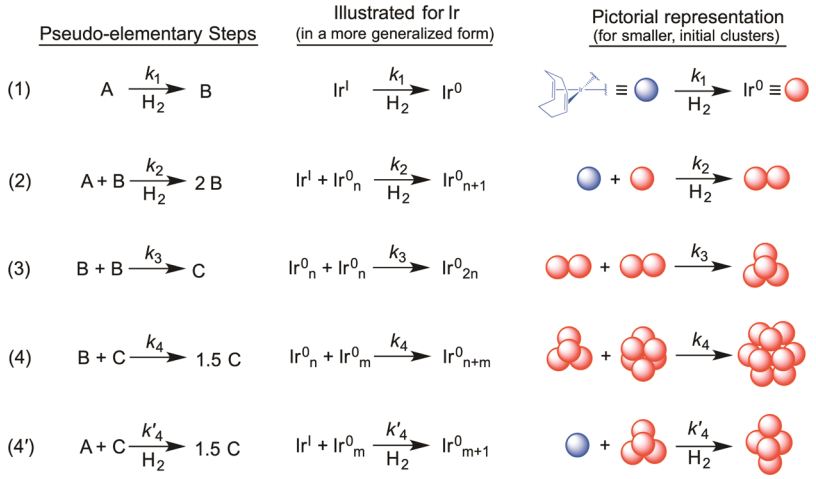

published in 2008.[56] In short, pseudo-elementary steps are a critical, but under-recognized and under-utilized, tool in dealing with the kinetics and underlying mechanisms of complex, multistep chemical reactions.

Shown in Scheme 3 are the two-step (steps (1) and (2)), three-step (steps (1), (2), and (3)), and two four-pseudo-elementary step (steps (1−4) or (1−3) and (4′)), deliberately minimalistic, Ockham's razor-obeying mechanisms for nanoparticle formation, worked out originally for $Ir(0)_n$ transition-metal nanoparticle formation.[5,18−23] Dihydrogen (H_2) is shown below the arrow where it is involved in the reaction. Nucleation is illustrated as unimolecular for simplicity and to be consistent the two-step mechanism[6] and the usage of these mechanisms in what follows. It should be noted, however, that bimolecular[4] as well as net termolecular nucleation[23] have been demonstrated in recent work.[7] Each mechanism is extensively disproof-based; for example, over 21 alternative mechanisms have been ruled out in formulation of the four-step mechanisms as documented elsewhere.[19−22] A new three-step mechanism has resulted from the ME-PBM studies,[7] namely steps (1), (2) + (3) (added, to become a single step), and (4′), as summarized in more detail in a later section.

1.6. Classical Approaches to Solving the PBM Equation. A paper by Falola and co-workers[57] gives an excellent overview of methods to solve PBEs. These can be divided into direct methods and methods of moments. The method of moments (MoM) (of "integral or summation averages") is a popular solution scheme for solving the general population balance model equation due to its comparatively low computational cost compared to other methods.[52,58−62] Moments, in this context, are averages over all particle sizes of powers of the PSD. Various powers/moments correspond, for example, to the number of particles, or the average or variance of the PSD. The MoM transforms the partial differential equation of the PBE into a series of ODEs for a select number of lower-order moments (e.g., 10 or fewer). This is an important point, as it teaches what one really wants is the full set of ODEs corresponding to the intimate mechanism, vide infra. However, sticking with the MoMs for the time being, these moments are then compared to experimental data, for example, the experimentally determined PSD.

However, because only a few moments are typically used, the crucial particle-size distribution generally cannot be computed in the absence of a moment-closure assumption such as assuming the shape of the PSD (see, however, ref 57 for an exception where the distribution can be obtained directly during simulation). The key point here is because the PSD intrinsically contains a summary of all of the kinetic events of the particle formation process(es), what one really wants to do is to fit the actual PSDs and their shape using simulations based on different mechanisms—which fits best, and why? We have been able to do just such fitting as a function of input mechanism(s) by a full ODE approach, vide infra.

In the standard PBM approach, particle size (which is, in reality, a discrete variable) is treated as a continuous variable for volume, V, and a partial differential equation (e.g., eq 2, vide supra) for particle number as a function of both time and V arises from the balance law expressed as eq 1, vide supra. This choice of a mathematically continuous variable V to express a physically discrete variable is known as a continuum approximation and allows one to express the balance law as one (partial) differential equation rather than a large system of ODEs, one equation for each discrete particle size. However, analytically solving the partial differential equation is, in general, not possible, and methods of numerically solving the equation rely on finding a system of ODEs that itself is an approximation (i.e., to the continuum approximation of the actual discrete entities). Thus, the direct or MoM approaches to (numerically) solve the partial differential equation are approximations of the continuum approximation to bring it back to a discrete system that can be solved numerically. These considerations are what led us to a full ODE approach as discussed next.

1.7. Full ODE Approach to the PBM in the Present Work: Resurrecting Smoluchowski's Classic 1918 Work. Reflection led us to make what has proved experimentally to be a very good choice in our approach to solving the PBM problem in the present work. We realized that instead of using ODE approximations of a partial differential equation (e.g., eq 2), that both much better and possible in our case would be to use the full system of ODEs corresponding to a near-atomistic account at the discrete kinetic level. In this way, we follow Smoluchowski's classic 1918 article,[63,64] in which he created a discrete model, in that classic case for particle agglomeration.

An important result of our full-ODE PBM which follows is, then, that it allows a rare, direct computation of the PSD shape from the ME-PBM, as well as curve-fitting of that predicted

https://dx.doi.org/10.1021/acs.jpcc.9b11239
J. Phys. Chem. C 2020, 124, 4852−4880

shape to the experimental PSD (i.e., rather than just a comparison of experimental data to moment-based averages). This approach is possible because the data we work with in this paper involves small enough particle sizes (particles consisting of up to $\sim 10^3$ monomers) so that the full, derived system of ODEs can be solved numerically in a reasonable amount of computation time (often $\lesssim$5 min for a single simulation) on a laptop computer, which translates to $\lesssim$10s of hours for the entire fitting process that might involve hundreds of individual simulations.

1.8. Disproof-Based Approach to the PBM in the Present Work. All of the ME-PBM work that follows is, as with the prior work leading to the minimum mechanisms used to enable the PBM,[6,18−25] performed with strict adherence to the preferred scientific method[16,17] of disproof of multiple alternative hypotheses. As Platt's classic paper notes "for exploring the unknown, there is no faster method".[17] The disproof-based nature of the PBM herein is, then and too, an important feature—actually a very important, somewhat rare feature in PBModeling—of our disproof-based ME-PBM approach.

2. EXPERIMENTAL SECTION

The primary details of the following sections were reported along with our first report[7] and hence need not be repeated here. However, for the convenience of the reader the following sections are reproduced in the Supporting Information of the present paper: S-V-1. Cyclohexene catalytic reporter reaction (CHCRR) kinetics; S-V-2. The PSD data; S-V-3. Measurement of K_{Diss} and k_{1alt}; S-V-4. Population balance modeling with PSD and CHCRR curve-fitting: resurrecting Smoluchowski's Classic 1918 full ODE approach to the PBM. A section on simulations and PSD curve-fitting is also given in context below as an aid to the reader and in support of our primary goal herein of making ME-PBM available to anyone that wishes to use it.

In the production of this full paper, a small error was found in one line of our original code:[7] the original version of the code had the POM mass balance equation using only k_2 instead of k_2 and k_3. Both the original and updated code can be found at https://github.com/drhandwerk/pbm; only the updated code is used herein. The one-line change in the code affects only the ME-PMB in Section 4.6 that uses the new three-step mechanism and also includes the experimental alternative termolecular mechanism.[23] The effect of the one-line change in the code is almost negligible on the fitted rate constants (in the second decimal point) as a look at the fitted rate constants in the prior[7] Figures 3 versus 17 herein reveal.

3. RESULTS AND DISCUSSION

3.1. Constructing the ODE Population Balance Model: Atomistic and Mathematical Interpretation of the Minimum Mechanisms in Scheme 1. As alluded to above, instead of modeling what is physically a discrete process in a continuous manner using a classic PBE (e.g., eq 2), and then discretizing the continuous problem to solve it, we chose to stay entirely in the discrete domain similar to the original Smoluchowski approach.[63,64] For larger particles, staying in the discrete domain is not computationally feasible, at least presently. However, the discrete domain, full ODE approach is feasible for the $Ir(0)_n$ nanoparticles studies herein that have an experimentally determined, maximum size of ca. 4 nm, corresponding to approximately 2500 atoms. The curve in Figure 1 is shown to ca. 3 nm, or 1000 atoms, but can be and was extrapolated to 4 nm = 2500 atoms.

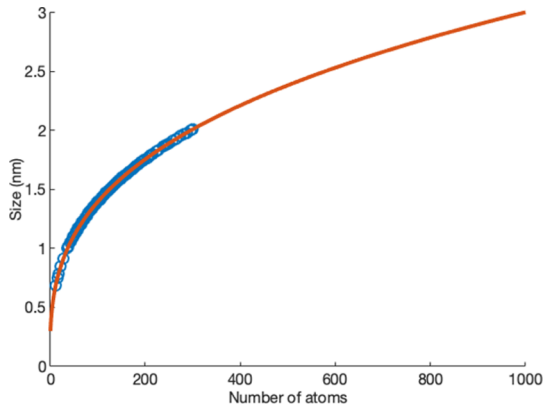

Figure 1. Plot showing the conversion between the particle diameter in nanometers and the number of atoms in an $Ir(0)_n$ particle. This figure was constructed using the formula that the number of atoms, n, in an Ir nanoparticle of diameter, d, is $n = (N_A\rho V)/MW_{Ir}$ where $N_A = 6.022 \times 10^{23}$ atoms/mol, the density of Ir is $\rho = 22.5$ g/cm^3, the volume $V = 4/3\pi(d/2)^3$, and the atomic weight of Ir (MW_{Ir}) = 192.2 g/mol. Blue circles are data; the red curve is the result of fitting the blue circles to the function $d(n) = 0.3000805n^{1/3}$. (Figure S1 of the Supporting Information provides an expanded look at the fit and other functions that were tried, but provided inferior fits, to the function shown). The resultant function is then used to convert the simulation results, which are in number of atoms, to diameter in order to compare to the experimental PSDs. Reprinted with permission from the Supporting Information of ref 7. Copyright 2019 American Chemical Society.

This approach does lead to a somewhat large (ca. 2500) system of ODEs, but one that is still easily solvable on current laptop/desktop hardware and one that allows us to both start and stay entirely within the discrete domain. Once we derive the particle interactions from the input mechanism, we can write our ODE system for the individual particle sizes. This process is equivalent to using a bin size of one in the various discretization methods for the PBE which, again, is typically not possible in applications of PBM to larger particle sizes.

The ODE systems are derived from the minimal mechanisms shown in Scheme 3 in an atomistic manner and starting (below) for the simplest, mechanism therein known as the Finke−Watzky (FW) two-step mechanism of A → B, then A + B → 2B.[6] While the A precursor (A = $\{(COD)Ir^{I}\cdot POM\}^{8-}$, Scheme 3) is well defined, conversion from the minimum mechanisms to the atomistic PBM requires defining what B and C (Scheme 3) are and otherwise specifying/interpreting the pseudo-elementary step[6,53] mechanisms atomistically and mathematically to get a system of ODEs that show how the numbers of particles of different sizes change with time. The conversion/interpretation is not unique, but (i) is far better than assuming a mechanism and use of inapplicable CNT for nucleation and (ii) is a disproof-based approach in which multiple different ME-PBModels can be—and are, in what follows—tested via curve-fits of the experimental PSD to each ME-PBM tested. Additionally, (iii) some variables in the ME-PBM, such as the integer M that defines the maximum "small" particle B and is the division point of the non-A particles B and C, can be—and again are, in what follows—treated as unknowns that can be determined via curve fitting.

https://dx.doi.org/10.1021/acs.jpcc.9b11239
J. Phys. Chem. C 2020, 124, 4852−4880

An example of atomistic interpretation of steps involving A, B, and C from Scheme 3 is given in Figure 2. Nucleation is known

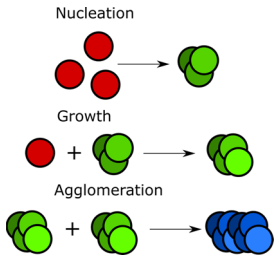

Figure 2. Illustration of A → B, A + B → 2B, and B + B → C pseudo-elementary steps in terms of initial atomistic particle interaction steps. A = red, B = green, and C = blue. Reprinted with permission from the Supporting Information of ref 7. Copyright 2019 American Chemical Society.

for the $Ir(0)_n$ nanoparticle formation system, and minimally involves[24] 2 to 3[23] Ir atoms as shown above for a possible termolecular nucleation, 3A → B_3. Growth is autocatalytic surface growth, so in the next step from B_3 is, then, A + B_3 → B_4. Bimolecular agglomeration (step (3) in Scheme 3) is then, atomistically, B_3 + B_3 → B_6, and so on for larger particle formations, where all possible (desired) reactions are considered in the ME-PBM. Using the law of mass action and the chosen interpreted mechanism yields a system of ODEs in terms of the precursor monomers, A. To facilitate comparison with experimental data, we first apply a simple change of variables to convert this system into a system of ODEs for particle size and then convert the particle size to particle diameter.

In what follows we will start with the simplest mechanism to enable the PBM and then slowly and deliberately add complexity as needed to better match the experimental PSD data. This approach couples an obeyance to Ockham's razor[65] with a disproof-based science[16,17] approach. The desired end result is a minimum mechanism able to explain nanoparticle formation while simultaneously disproving other possible, conjectured mechanisms based on Scheme 1. Adding complexity can, in turn, reveal changes if not *simplifications* that should be made in the postulated mechanism. Indeed, we will see an example of this—one solution to the specific inverse problem here—where the "effects" (the PSD) feeds back into and corrects the mechanism (i.e., the "cause") leading to those effects via the tool of the ME-PBM. Specifically, a new, three-step mechanism,[7] which is simpler than a four-step mechanism that was being considered yet accounts nicely for the PSD, is detailed in what follows.

3.2. Six of Twelve Specific Mechanisms Tested and Their Associated ME-PBModels. Six specific mechanisms are presented below, built from the two-step, a four-step (steps (1), (2), (3), and (4′) in Scheme 3), and a new three-step mechanism that resulted from the PBM analysis (vide infra). Each of the above three primary mechanisms examined is PBModeled with simple termolecular nucleation to start and then with the experimentally determined alternative-termolecular nucleation; hence, a total of six mechanisms are examined below by ME-PBModeling. En route to these six illustrative cases selected for the main text, we also tested simple unimolecular nucleation, bimolecular nucleation, fourth-order nucleation (following a literature PBM[52]), the classic three-step mechanism back in (steps (1) through (3) in Scheme 3), a second four-step mechanism (steps (1) through (4) in Scheme 3), and a 5-step mechanism with all of the steps in Scheme 3. The results for these additional six PBMs are summarized in the Supporting Information, Figures S2−S7, for the interested reader. Hence, a total of 12 mechanisms and associated PBModels were tested en route to the 6 disproof-based PBModels selected for presentation below.

3.2.1. Original FW Two-Step Mechanism.[7] In this section, we first create each of the six ME-PBModels that will be presented and then in a separate section give the results of the simulations and curve-fitting comparisons to the experimental PSDs.

The first mechanism we examined[7] is the FW two-step mechanism shown as the first two steps (1) and (2) back in Scheme 3, pseudo-elementary steps reproduced below as eq 3 consisting of slow, continuous nucleation and then autocatalytic (surface) growth[6]

$$\mathrm{A} \xrightarrow{k_1} \mathrm{B}$$
$$\mathrm{A} + \mathrm{B} \xrightarrow{k_2} 2\mathrm{B} \tag{3}$$

3.2.1.1. Derivation of the Two-Step, Mechanism-Enabled PBM.[7] First, some required notation: let the concentration (in moles/liter) of precursor monomers be denoted by m_1. The concentration of particles of size j (i.e., the concentration of particles that consist of j monomers) is denoted by n_j. The collection of particles of size j therefore contains a total of jn_j monomers per unit volume. Our differential equations will initially be written in terms of this total concentration of monomers that are contained in particles of a given size j, denoted by $m_j = jn_j$. Hence, the concentration of precursor monomers (not contained in any particle) may also be written as m_1. The concentration of binding sites on a particle of size j will be known as b_j. The relationship between the total concentration of monomers in particles of size j and the concentration of those that are available to bind is given by the relationship $b_j = r(j)m_j$, where the (dimensionless) function $r(j)$ can represent various effects such as volume- or surface-area- dependent growth,[6] or ligand capping.[54,55] Indeed, if we define a new function $\hat{r}(j) = k_i r(j)$ then this new function represents all growth processes for a particle of size j and is called the growth kernel. In what follows, we keep the rate constants k_i and the function $r(j)$ explicit.

Unlike the PBE, which has no direct particle−particle interactions, our model is based on atom-to-atom contact. As such, the monomers on the particle surface should be capable of binding while those on the inside remain unreactive. Therefore, a surface area model is adapted by choosing the function $r(j) = 2.677j^{0.72}/j$. This is the number of surface monomers divided by the total number of monomers, where the number of surface atoms is taken from Schmidt and Smirnov[66] and where the natural number j represents the particle size.

3.2.1.2. Third-Order Nucleation. In the present case of Ir(0) nanoparticle formation, it is known experimentally[23] that nucleation is nominally third-order and hence nominally termolecular in Ir, written as 3A → 3B (=B_3), neglecting for the moment the additional kinetic details of the alternative-termolecular nucleation mechanism shown back in Scheme 2 and associated prior equilibria needed to achieve a "termolecular" reaction,[23] true termolecular reactions being well demonstrated only in the gas phase. Consistent with and fully supportive of net Ir_3 termolecular nucleation, lower first- and second-order nucleation, A → B and 2A → 2B, respectively, were found to provide inferior fits to the PSD as detailed in the Supporting Information. Noteworthy here is the simplification

https://dx.doi.org/10.1021/acs.jpcc.9b11239
J. Phys. Chem. C 2020, 124, 4852−4880

afforded by correctly mechanistically enabling the PBM with an experimentally determined nucleation mechanism. All lower as well as higher order (i.e., greater than 3) nucleation pathways need not be considered because they have been ruled out experimentally. Hence all the PBModels that follow (i) will be based on termolecular nucleation in Ir (i.e., Ir_3) as one minimum complexity model (and although we will refer to that net 3A → 3B (=B_3) step as the reduced "A → B, rate constant k_1, for convenience in what follows), and then (ii) a set of PBModels will be constructed where the actual experimentally determined alternative termolecular nucleation is fully implemented.

As we first noted in our 2019 paper,[7] to describe the reactions and differential equations, we will use the notation n_j to refer to particles of size j and also use n_j as the variable to denote the concentration of such particles as was also described above. Similarly, we will use the notation m_j to refer to monomers contained in particles of size j as well as the variable to denote the concentration of such particles as described above. (It is to be understood in what follows that where we say "monomer" or "particle" we are referring to the concentration of monomers and concentration of particles in units of moles/liter = molarity which allows the results of the ME-PBM to be compared to the experimental data).

Starting then with simple third-order nucleation, this nucleation can be written in terms of the monomer, m_1, that are converted into "monomer" units m_3, three of which make up one particle nucleus n_3

$$3m_1 \overset{k_1}{\rightarrow} 3m_3 (= 1n_3) \tag{4}$$

Note that in the above notation 3 m_1 precursors form a particle of size 3 (i.e., 1 n_3) which still contains the 3 monomers, now called m_3. Growth of the nucleus is modeled by $m_1 + m_3 \overset{k_2}{\rightarrow} 2m_4 - 2m_3 + 2m_4$ and in general, growth is $m_1 + m_j \overset{k_2}{\rightarrow} 2m_{j+1} - (j-1)m_j + (j-1)m_{j+1}$ for a particle of size j. The left hand side of these growth relationships indicates that a single precursor monomer will interact with a single monomer that is part of a larger particle, as visualized in Figure 3. Physically we know that the internal atoms are not available to directly bind and interact with the precursor at the atomistic level, which in turn is the primary reason for the adoption of surface-area growth in this paper. The right hand side of the relationships is the results of the monomer−particle interaction. The first term represents the precursor and the particle monomer becoming monomers of a particle of size one larger, the middle term is the loss of the rest of the original monomers, and the final term is the rest of the original monomers changing to the larger size. Combining terms, we have the result

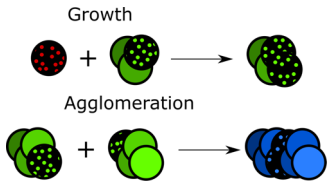

Figure 3. Illustration of how particle interaction steps are specified/interpreted atomistically in the ME-PBM model derivation. The dotted atoms are those which are actually interacting. Autocatalytic growth, formally A + B → 2B, has the red-dotted atom joining with the green-dotted which makes two green-dotted atoms. Also shown above is bimolecular agglomeration, formally B + B → C, that has the two green-dotted atoms combining to make two blue-dotted C atoms. This coalescence step also has the effect of changing the solid green atoms into solid blues, which will be shown to be important in the following section (vide infra). Reprinted with permission from the Supporting Information of ref 7. Copyright 2019 American Chemical Society.

$$m_1 + jm_j \overset{k_2}{\rightarrow} (j+1)m_{j+1} \tag{5}$$

which says that the addition of a precursor monomer to a particle with j monomer units will form a new particle with $j + 1$ monomer units.

Taking relations 4 and 5, and noting that the precursor a only attaches to binding sites leads to the equations for changes in monomers where $j \geq 4$. (Note that we write the positive derivative, $+dm_1/dt$, which means that the loss terms in the precursor a are proceeded by a minus sign).

$$\begin{aligned}
\frac{dm_1}{dt} &= -3k_1{m_1}^3 - k_2m_1\sum_{j=3}^{\infty} b_j \\
\frac{dm_3}{dt} &= 3k_1{m_1}^3 - 3k_2m_1b_3 \\
\frac{dm_j}{dt} &= jk_2m_1(b_{j-1} - b_j)
\end{aligned} \tag{6}$$

This system must now be converted into a system for the particles n_j using the $m_j = kn_j$ and $b_j = r(j)m_j$ substitutions described above. These give (while noting that the differential equations that follow are written with a positive sign on the left, dn/dt side)

$$\begin{aligned}
\frac{dn_1}{dt} &= \underbrace{-3k_1{n_1}^3}_{\text{loss from nucleation}} \underbrace{-k_2n_1\sum_{j=3}^{\infty} r(j)jn_j}_{\text{loss from growth}} \\
\frac{dn_3}{dt} &= \underbrace{k_1{n_1}^3}_{\text{gain from nucleation}} - \underbrace{3k_2n_1r(3)n_3}_{\text{loss from growth}} \\
\frac{dn_j}{dt} &= \underbrace{k_2n_1((j-1)r(j-1)n_{j-1} - jr(j)n_j)}_{\text{gain and loss from growth}}
\end{aligned} \tag{7}$$

From here, we see that if the growth rate k_2 is taken to be a function of size, instead of a constant, then it would have to be distributed into the sum and difference. This would give the kernel $k_2(j)r(j)$, consistent with our previous definition of $\hat{r}$, the growth process kernel. Simulations and PSD summarized in the next section will reveal that the two-step mechanism is incapable of matching the experimental particle-size distribution. Hence, more complex models were developed, the best fitting of which, at least initially, proved to be the four-step model developed next.

3.2.2. Four-Step Mechanism. The mechanism-enabled four-step PBModel was developed post the two-step mechanism and also post the six other specific mechanisms considered in the Supporting Information. The experimental basis and support for the following four-pseudo-elementary step mechanism are available in a 2014 paper for the interested reader.[22]

https://dx.doi.org/10.1021/acs.jpcc.9b11239
J. Phys. Chem. C 2020, 124, 4852−4880

$$\begin{aligned} &A \xrightarrow{k_1} B \\ &A + B \xrightarrow{k_2} 2B \\ &B + B \xrightarrow{k_3} C \\ &A + C \xrightarrow{k_4} 1.5C \end{aligned} \tag{8}$$

The four steps consist of slow, continuous nucleation, autocatalytic surface growth, bimolecular agglomeration, and what is termed secondary autocatalytic surface growth.[22] This mechanism introduces a third particle species, C, representing "large" particle sizes. Coding this four-step mechanism emphasizes the specification/interpretation required to go between the pseudo-elementary step mechanism and the PBModel. The monomer-addition growth process is now two separate steps, one for the "small" B particles and one for the "large" C particles (the dividing line between B and C being designated by M, a fit variable in the code, vide infra). This splitting of B and C is implemented as a step-function approximation of monomer growth (as also done in the mechanism in upcoming eq 11, vide infra), but we also have now agglomeration in the model in the form of the B + B step. This says that two "small" particles may interact, but that if a particle is too large, it will only grow from monomer growth. Only allowing the smaller particles to agglomerate is in line with our minimal extension, Ockham's razor approach[65] and the notion that more complex models can always be built and tested.

It is also necessary to fix the ambiguity in the mechanism of what B and C mean when building the atomistic ODE model in the code for this still-by-design minimalistic (i.e., Ockham's razor obeying) mechanism and associated minimalistic ME-PBM. This was done by choosing a cutoff for the largest B size: let the natural number M be the largest B size. Hence, we have explicit sizes for the two species given by $B = \{n_j | j \le M\}$ and $C = \{n_j | j > M\}$. That is, all sizes less than or equal to the cutoff size n_M are of species B, and all larger sizes are of species C. This distinction between B and C can be (and was) fit for during the PSD-fitting process (i.e., M was treated as a fit parameter, vide infra). Note that other than the B versus C cut-off parameter, M, mechanisms with either A + B → 2B or A + B → C steps are the same as far as the code is concerned (because $n_1 + n_j$ goes to n_{j+1}, which means that it doesn't matter in if n_{j+1} is called "B" or "C"). Note also that the $n_1 + n_j \rightarrow n_{j+1}$ step is formally autocatalytic, as the product n is also a reactant. That is, as coded both the A + B → 2B versus A + B → C steps are formally autocatalytic.

3.2.2.1. Derivation of the Four-Step Mechanism Enabled PBM. The derivation of the four-step and all other PBMs herein is similar to the two-step derivation and includes termolecular ($3A \rightarrow A_3$) nucleation to start and unless stated otherwise. We start with specifying/interpreting the mechanism to make the concepts of B and C well defined by using the definitions given in the above paragraph, as must be done to convert the mechanism into a system of ODEs. The four-step mechanism says that two "small" particles B agglomerate into one "large" particle C as shown schematically at the atomic level back in the third step of Figure 2. However, two small particles may also form another small particle. For example, if the cutoff between small and large is say $M = 40$, two particles of 15 will agglomerate to form a 30 which is still a "small" particle in this example. Our implementation of the PBModel from the mechanism, while again not unique at this stage, is a fair interpretation of the mechanism and captures its main ideas at the atomistic level—the essence of ME-PBM. Interesting here is that experimental[67] as well as computational evidence and literature (for Ir_{48})[68] imply that at least unligated, naked $Ir(0)_{\sim 40-50}$ exhibit a somewhat enhanced stability and hence higher kinetic barrier to agglomeration.

Hence and because there is neither a B + C nor a C + C term in this particular four-step mechanism, agglomeration only involves "small"−"small" particle interaction. Let the growth rate function be expressed as eq 9.

$$k_g = \begin{Bmatrix} k_2 \text{ if "small"} \\ k_4 \text{ if "large"} \end{Bmatrix} \tag{9}$$

with the inclusion of agglomeration, and for third-order nucleation to start, the ODE system, written in terms of monomers m_j, becomes as shown in eq 10

$$\begin{aligned}
\frac{dm_1}{dt} &= -3k_1 m_1^3 - m_1 \sum_{k=3}^{\infty} k_g b_k \\
\frac{dm_3}{dt} &= 3k_1 m_1^3 - 3k_2 m_1 b_3 - 3k_3 b_j \sum_{k=3}^{M} b_k \\
\frac{dm_{4,5}}{dt} &= jk_2 m_1 (b_{j-1} - b_j) - jk_3 b_j \sum_{k=3}^{M} b_k \\
\frac{dm_j}{dt} &= jk_2 m_1 (b_{j-1} - b_j) - jk_3 b_j \sum_{k=3}^{M} b_k + jk_3 \sum_{\substack{i=0 \\ \lfloor j/2 \rfloor - i \ge 3 \\ \lfloor j/2 \rfloor + i + (j \bmod 2) \le \infty}}^{\infty} b_{\lfloor j/2 \rfloor - i} b_{\lfloor j/2 \rfloor + i + j \bmod 2}, \qquad 6 \le j \le M \\
\frac{dm_{M+1}}{dt} &= (M+1) m_1 (k_3 b_M - k_4 b_{M+1}) + jk_3 \sum_{\substack{i=0 \\ \lfloor (M+1)/2 \rfloor - i \ge 3 \\ \lfloor (M+1)/2 \rfloor + i + ((M+1) \bmod 2) \le \infty}}^{\infty} b_{\lfloor (M+1)/2 \rfloor - i} b_{\lfloor (M+1)/2 \rfloor + i + (M+1) \bmod 2} \\
\frac{dm_l}{dt} &= lk_4 m_1 (b_{l-1} - b_l) + jk_3 \sum_{\substack{i=0 \\ \lfloor j/2 \rfloor - i \ge 3 \\ \lfloor j/2 \rfloor + i + (j \bmod 2) \le \infty}}^{\infty} b_{\lfloor j/2 \rfloor - i} b_{\lfloor j/2 \rfloor + i + j \bmod 2}, \qquad M + 2 \le l < \infty
\end{aligned} \tag{10}$$

The smallest particle formed by agglomeration is 6, which

https://dx.doi.org/10.1021/acs.jpcc.9b11239
J. Phys. Chem. C 2020, 124, 4852−4880

occurs when two nuclei combine. The equation for m_j gives the changes in time of the numbers of particles that can be both created and lost via agglomeration. The equation for m_l gives the change in time of the number of particles that can be formed via agglomeration, at least up twice the maximum j size, but that cannot be lost to agglomeration because there are no "small"−"large" or "large"−"large" interactions.

Using the same $m_j = jn_j$ and $b_j = r(j)m_j$ substitutions as for the two-step mechanism, we transform the monomer system into the following system for particle size

$$
\begin{aligned}
\frac{dn_1}{dt} &= \underbrace{-3k_1n_1^3}_{\text{loss from nucleation}} \underbrace{- n_1\sum_{k=3}^{\infty} k_g r(k) k n_k}_{\text{loss from growth}} \\
\frac{dn_3}{dt} &= \underbrace{k_1n_1^3}_{\text{gain from nucleation}} \underbrace{- k_2n_1r(3)3n_3}_{\text{loss from growth}} \underbrace{- k_3r(3)3n_3\sum_{k=3}^{M} r(k)kn_k}_{\text{loss from agglomeration}} \\
\frac{dn_{4,5}}{dt} &= \underbrace{k_2n_1\big(r(j-1)(j-1)n_{j-1} - r(j)jn_j\big)}_{\text{gain and loss from growth}} \underbrace{- k_3r(j)jn_j\sum_{i=3}^{M} r(i)in_i}_{\text{loss from agglomeration}} \\
\frac{dn_j}{dt} &= \underbrace{k_2n_1\big(r(j-1)(j-1)n_{j-1} - r(j)jn_j\big)}_{\text{gain and loss from growth}} \underbrace{- k_3r(j)jn_j\sum_{i=3}^{M} r(i)in_i}_{\text{loss from agglomeration}} \\
&\quad \underbrace{+ k_3\sum_{\substack{i=0\\ \mu\geq 3\\ \nu\leq M}}^{\infty} r(\mu)\mu n_\mu r(\nu)\nu n_\nu}_{\text{gain from agglomeration}}, \qquad 6 \leq j \leq M \\
\frac{dn_{M+1}}{dt} &= \underbrace{n_1\big(k_2r(M)Mn_M - k_4r(M+1)(M+1)n_{M+1}\big)}_{\text{gain and loss from growth}} + \underbrace{k_3\sum_{\substack{i=0\\ \mu\geq 3\\ \nu\leq M}}^{\infty} r(\mu)\mu n_\mu r(\nu)\nu n_\nu}_{\text{gain from agglomeration}} \\
\frac{dn_l}{dt} &= \underbrace{k_4n_1\big(r(l-1)(l-1)n_{l-1} - r(l)ln_l\big)}_{\text{gain and loss from growth}} + \underbrace{k_3\sum_{\substack{i=0\\ \mu\geq 3\\ \nu\leq M}}^{\infty} r(\mu)\mu n_\mu r(\nu)\nu n_\nu}_{\text{gain from agglomeration}}, \qquad M+2 \leq l < \infty.
\end{aligned}
\tag{11}
$$

In these equations, $\mu = \left|\frac{j}{2}\right| - i$ and $\nu = \left|\frac{j}{2}\right| + i + (j \bmod 2)$, respectively, and M is the cutoff between the small particles B and the large particles C. The value M also serves as the cutoff for which particles agglomerate because the class of large particles does not agglomerate in this model due to the lack of B + C or C + C steps. The j sizes are both formed and consumed by the agglomeration process. The l sizes are larger than the maximum agglomeration size M and therefore cannot be consumed by agglomeration, but may potentially still be formed via agglomeration.

The sums representing the gains from agglomeration in eq 11 are best explained with an example. Say that $j = 50$. The μ and ν particles that interact would be 25 + 25, 24 + 26, and so on until the left number μ reaches 3, or the right number ν reaches M. The sum will always stop with the $\mu \geq 3$ condition for B-sized particles. For the larger C size particles the $\nu \leq M$ condition is necessary. For example, if $l = 100$ and $M = 40$, we have that n_{100} cannot be formed from the combination of two n_{50}'s because $50 > M$ and only particles smaller than M are agglomerating in this model.

3.2.3. New Three-Step Mechanism Resulting from the PBModeling.[7] As recently reported,[7] what proved to provide a better fitting ME-PBM is the new three-step mechanism, shown below in eq 12, which is a reduction of the four-step mechanism in eq 8 in which the middle two steps of small-particle growth and small−small particle agglomeration are combined. Specifically, the growth step in the above four-step mechanism is A + B → 2B, while the agglomeration step is B + B (=2B) → C; the resulting combination from simply adding these two steps is then A + B → C. The idea that this single, combined pseudo-elementary step might work (while also reducing one adjustable parameter in the model) became apparent as the PBModeling proceeded, specifically from the finding that the k_3 rate constant for the B + B → C step of the four-step mechanism back in eq 8 often came out near zero when there was no lower bound set during the fitting process. This suggests that agglomeration per se is kinetically unimportant in the present $Ir(0)_n$ nanoparticle formation system. Additionally, it led us to consider dropping the B + B (=2B) → C and also A + B → 2B steps and adding in their place monomer growth to form C (i.e., A + B → C), as summarized in eq 12 below. The agglomeration step, for example 4 + 4 = 8, which moves more particle mass to the right faster, can be thought of as monomer growth, that is, as 3 + 1+1 + 1+1 + 1 = 8, with perhaps an increased rate constant.

$$
\begin{aligned}
&\mathrm{A} \xrightarrow{k_1} \mathrm{B} \\
&\mathrm{A} + \mathrm{B} \xrightarrow{k_2} \mathrm{C} \\
&\mathrm{A} + \mathrm{C} \xrightarrow{k_3} 1.5\mathrm{C}
\end{aligned}
\tag{12}
$$

The new three-step mechanism can be thought of as a one-step extension of the classic FW two-step mechanism,[6] but one

https://dx.doi.org/10.1021/acs.jpcc.9b11239
J. Phys. Chem. C 2020, 124, 4852−4880

where instead of having a constant growth rate for particles of all sizes, small and large particles are allowed to grow with different rates—and with a step-function growth kernel from k_2 to k_3. This new three-step mechanism, discovered as the PBModeling proceeded, is an important finding of the present ME-PBM efforts. The appropriate system of ODEs follows analogously to those presented so far and are provided in the Supporting Information.

3.2.4. Two-Step Mechanism with Alternative Termolecular Nucleation. Compelling experimental support for the "alternative termolecular mechanism" given in Scheme 2 was published in 2017.[23] That kinetic and other data included a quantitative fit to the expected inverse, quadratic-root dependence on added POM for this mechanism. The resultant K_{Diss} (Diss = dissociation) equilibrium constant obtained from that kinetics data agreed quantitatively within experimental error with an independently measured[23] $K_{Diss,\ apparent} = K_{Diss}[Solvent]^2 = (6.4 \pm 1.4) \times 10^{-5}$ M and, accordingly, $K_{Diss} = 5 \times 10^{-7}$ M^{-1} for the mixture of 2.5 mL acetone solvent and 0.5 mL cyclohexene, hence [Solvent] = 11.3 M. The important, state-of-the-art point for the ME-PBM is that we not only know the (experimentally determined) nucleation mechanism so it can be input as a known part of the ME-PBM, but we also have the K_{Diss} value as an experimentally determined constraint for the curve-fitting of the PSD. In other words, ME-PBM entails putting each and every available piece of mechanistic and other experimental information one has (such as known equilibrium or rate constants) into the ME-PBM being tested.

The basic two-step mechanism described by the kinetic eq 3 becomes the system in eq 13 with the replacement of the A → B nucleation step by the experimentally determined alternative termolecular nucleation[23] in this important, first case of known-nucleation mechanism-enabled PBModeling, with K_{Diss} being an abbreviation for $K_{Dissociation}$

$$
\begin{aligned}
&2[A + 2S \rightleftharpoons A_{solv} + POM],\\
&\quad K_{Diss}\ \text{equilibrium constant}\\
&2A_{solv} + A \xrightarrow{k_{1alt}} 3B + POM + 4S\\
&A + B \xrightarrow{k_2} 2B + POM
\end{aligned}
\tag{13}
$$

The three new species involved are the ligand, POM, the $A_{solv} = \{(COD)Ir^{I}\cdot(solvent)_2\}^{+}$ and the solvent, S. Note that, as the reaction proceeds, the POM ligand that is freed from the $A = \{(COD)Ir^{I}\cdot POM\}^{8-}$ precursor (i.e., the POM that is not bound to the B = Ir(0) nanoparticle surface) can shift the dissociation equilibrium back to the left, thereby serving to slow down nucleation.

The ODE system for the number of particles in this ME-PBM is

$$
\begin{aligned}
\frac{dn_1}{dt} &= \underbrace{-k_{1alt}n_1{n_s}^2}_{\text{loss from nucleation}} \underbrace{-k_2n_1\sum_{j=3}^{\infty} jr(j)n_j}_{\text{loss from growth}} \underbrace{-k_{+k_{Diss}}n_1s^2 + k_{-k_{Diss}}n_sp}_{\text{fast dissociation step}}\\
\frac{dn_s}{dt} &= \underbrace{k_{+k_{Diss}}n_1s^2 - k_{-k_{Diss}}n_sp}_{\text{fast dissociation step}} - \underbrace{2k_{1alt}n_1{n_s}^2}_{\text{loss from nucleation}}\\
\frac{dp}{dt} &= \underbrace{k_{+k_{Diss}}n_1s^2 - k_{-k_{Diss}}n_sp}_{\text{fast dissociation step}} + \underbrace{k_{1alt}n_1{n_s}^2}_{\text{gain from nucleation}} + \underbrace{k_2n_1\sum_{j=3}^{\infty} jr(j)n_j}_{\text{gain from growth}}\\
\frac{dn_3}{dt} &= \underbrace{k_{1alt}n_1{n_s}^2}_{\text{gain from nucleation}} - \underbrace{k_2n_1r(3)3n_3}_{\textit{loss}\ \text{from growth}}\\
\frac{dn_j}{dt} &= \underbrace{k_2n_1(r(j-1)(j-1)n_{j-1} - r(j)jn_j)}_{\text{gain and loss from growth}}
\end{aligned}
\tag{14}
$$

with the new species n_s representing A_{solv} and p representing POM.

3.2.5. Four-Step Mechanism with Alternative-Termolecular Nucleation. The four-step mechanism with alternative nucleation is

$$
\begin{aligned}
&2[A + 2S \rightleftharpoons A_{solv} + POM], \qquad K_{Diss}\ \text{equilibrium constant}\\
&2A_{solv} + A \xrightarrow{k_{1alt}} 3B + POM + 4S\\
&A + B \xrightarrow{k_2} 2B + POM\\
&B + B \xrightarrow{k_3} C\\
&A + C \xrightarrow{k_4} 1.5C + POM
\end{aligned}
\tag{15}
$$

The alternative-termolecular four-step has the same nucleation steps as the standard four-step as well as the small−small agglomeration k_3 step. In contrast, the growth steps are split into small, k_2, and large, k_4, growth. As with the standard four-step, free POM is created whenever the precursor A is involved in a step. The appropriate system of ODEs is provided in the Supporting Information.

3.2.6. New Three-Step Mechanism with Alternative-Termolecular Nucleation. The new three-step mechanism with alternative-termolecular nucleation is

$$
\begin{aligned}
&2[A + 2S \rightleftharpoons A_{solv} + POM],\\
&\quad K_{Diss}\ \text{equilibrium constant}\\
&2A_{solv} + A \xrightarrow{k_{1alt}} 3B + POM + 4S\\
&A + B \xrightarrow{k_2} C + POM\\
&A + C \xrightarrow{k_3} 1.5C + POM
\end{aligned}
\tag{16}
$$

The ME-PBModel from this mechanism now has the correct nucleation steps and, as will be shown below, is the best at reproducing the experimental size distributions out of the 12 total mechanisms examined. The appropriate system of ODEs is provided in the Supporting Information. As noted in the

https://dx.doi.org/10.1021/acs.jpcc.9b11239
J. Phys. Chem. C 2020, 124, 4852−4880

Experimental Section, the code is freely available at https://github.com/drhandwerk/pbm.

4. SIMULATIONS AND PSD CURVE-FITTING

The ODE system models of the mechanisms in the previous section were coded in MATLAB. See the Experimental section in the Supporting Information.

The ODEs are in terms of particle size while the experimental data are grouped (binned) into particles of similar diameter in nanometers, as for example in Figure 4. To compare the simulations to experiment a conversion function was needed, and $d(n) = 0.3000805n^{1/3}$ as determined in Figure 1 (vide supra) was used. Others were also tested but resulted in poorer fits; see Figure S1 of the Supporting Information.

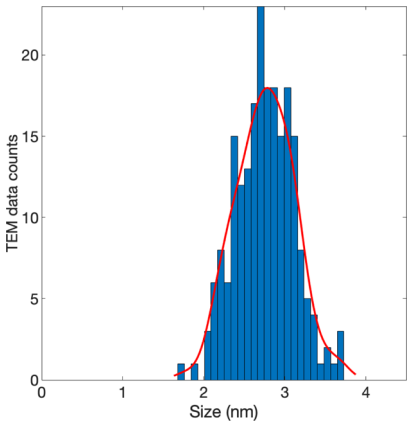

Figure 4. TEM-determined, experimental PSD histogram, in blue, for $Ir(0)_n$ nanoparticles prepared from 1.2 mM $\{(1,5\text{-COD})Ir^{I}\cdot POM\}^{8-}$ in acetone at 22 °C under 40 psig initial H_2 pressure and at 4.838 h. The red curve is a fit to the histogram using MATLAB's histfit function that, in turn, will be used to compare to the simulated, normalized PSDs for each ME-PBM. The red curve is extended with zeros on the left and right of the histogram to the complete simulation size domain, interpolated with griddedInterpolant, and normalized to have a maximum of one. The ∼2.7 nm average size of the Ir(0) particles corresponds to an approximately $Ir(0)_{\sim 730}$ nanoparticles. Reprinted with permission from the Supporting Information of ref 7. Copyright 2019 American Chemical Society.

Unless otherwise noted, all simulations were carried out using MATLAB, and fits to the experimental PSD were performed using the fitting function pattern search, which allows for multivariate constrained fitting. To compare the simulations to the experimental histograms, MATLAB's histfit function with the kernel option was used on the transmission electron miscoscopy (TEM)-determined histograms to obtain a smooth fit that provides a continuous approximation of the PSD, as shown in Figure 4.

This fit to the TEM-determined PSD and the simulation PSD were normalized and interpolated with griddedInterpolant to be on the same domain grid. The objective function supplied to patternsearch was the L_1-norm, given by $\|V\| = \sum|V_j|$ of the difference V of the histfit-supplied PSD and the simulated PSD at the fourth and final experimental time step of 4.838 h (the experimental times were recorded originally in seconds and, hence, are precise to ±0.005 h). In the figures below, the TEM histogram and the simulation PSDs are overlaid, the shape of the two graphs being what was minimized and, hence, what is emphasized. The vertical axes necessarily have different units as shown. The objective function for the CHCRR fits is the L_2-norm $\|V\| = (\sum|V_j|^2)^{1/2}$ of the difference between the CHCRR curve and the simulated precursor concentration. Each of these L_p-norms gives the best function value (BFV) listed in the figures below. Because fits to the CHCRR and the final histogram use different norms, one needs to keep in mind that the respective BFVs from the CHCRR and histograms fits are not directly comparable.

A comparison was also done to see how closely the simulated PSD or the precursor loss kinetics curve compare to the experimental PSD or the cyclohexene hydrogenation catalytic reporter reaction (CHCRR) kinetics curve.

Because the PSD is information rich, fits to the PSD are what we will emphasize in what follows, even though we may often start with the quicker fit to the CHCRR kinetics curve—and then use the rate constants from the CHCRR fit as the first simulation to compare to the TEM results. But and again, because of the assumptions behind the CHCRR and, hence, its lack of reliability past the first ca. one-third to one-half of the CHCRR kinetics curves,[4,6,18−22] the fits to the TEM histograms are once again what we wish to emphasize in what follows.

4.1. Two-Step ME-PBM. The two-step ME-PBM results are shown in Figures 5−7. Keep in mind that unless stated otherwise, the PBModels that follow include termolecular nucleation (and, hence, the units for the k_1 rate constant are M^{-2} h^{-1}). The two-step PBM is capable of matching the CHCRR curve (Figure 5); however, the two-step fails to produce an accurate PSD, whether the fit is to the CHCRR curve, or to the histograms. The distributions produced by the two-step ME-PBM have too small a mean. The apparent physical picture from this simplest, hence initial, PBM is that the smaller size particles are either being produced too quickly, or being consumed too slowly, in the two-step model.

Fits from Figure 8 on will employ only the fourth, 4.838 h, final PSD due to (i) the lack of improvement from fitting to all four histograms rather than just the last, fourth histogram, and (ii) the inability at least presently to correctly weight/prioritize each of the four histograms when trying to fit all four simultaneously.

The bottom line from the attempt to account for primarily the PSD histograms as a function of time using the simplest, two-step ME-PBModel with termolecular nucleation is that the classic FW two-step mechanism is unable to account for the experimental PSD data, even when expanded to include termolecular nucleation (Figures 5−7). A similar conclusion was reached from a MoM approach PBM while employing just the FW two-step mechanism.[52] Unfortunately, that prior attempt at PBM was not enabled by knowledge of the nucleation mechanism nor did it employ the necessary disproof-based method as employed herein of testing all currently possible minimum ME-PBMs.[52] As a result, that study reached the erroneous conclusion[52] that "a delayed onset of nucleation and its suppression soon after..."[52] is the key to accounting for the observed, experimental PSD. This prior assertion[52] will be shown to be incorrect and quite misleading, based on the findings of the present mechanism-enabled PBM, vide infra.

An important point in this regard is that, comparing Figures 5−7 (that are based on models with termolecular nucleation) to the attempted curve-fits in the Supporting Information (using unimolecular or bimolecular nucleation) reveals that better approximations to the experimental PSDs are obtained (and in all cases herein, as it turns out) by using the experimentally established nucleation mechanism that involves three iridium, Ir_3. This finding strongly supports both the experimentally

https://dx.doi.org/10.1021/acs.jpcc.9b11239
J. Phys. Chem. C 2020, 124, 4852−4880

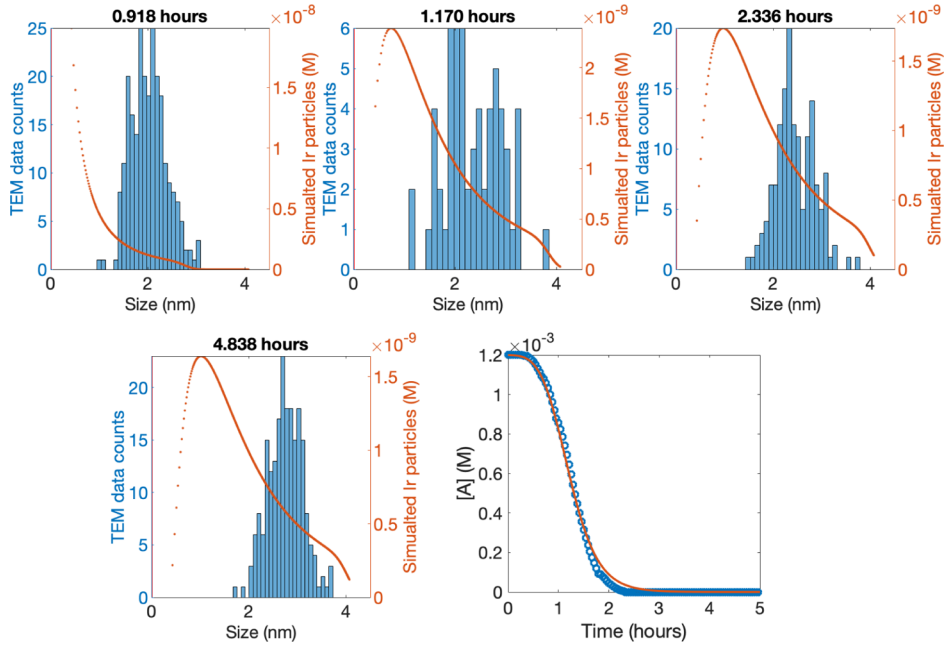

Figure 5. Attempted two-step with third-order nucleation ME-PBM fit of the CHCRR curve to start using MATLAB's fminsearch. The parameters obtained from the CHCRR fitting process are the rate constants $k_1 = 9.14 \times 10^2$ M^{-2} h^{-1}, $k_2 = 6.70 \times 10^3$ M^{-1} h^{-1}. The BFV is 2.48×10^{-4} (the much smaller, ca. 10^{-4} BFV being typical for fits to the CHCRR compared to the generally higher BFVs seen for fits to the PSD, vide infra). Recall that the "k_1" value here is by our earlier definition the rate constant for the implemented net termolecular nucleation in this (and several subsequent) ME-PBMs, as recognizable by its units of M^{-2} h^{-1}. The rate constant parameters from the CHCRR fit were then used to generate the PSD fits shown for the first, 0.918 to final, 4.838 PSDs.

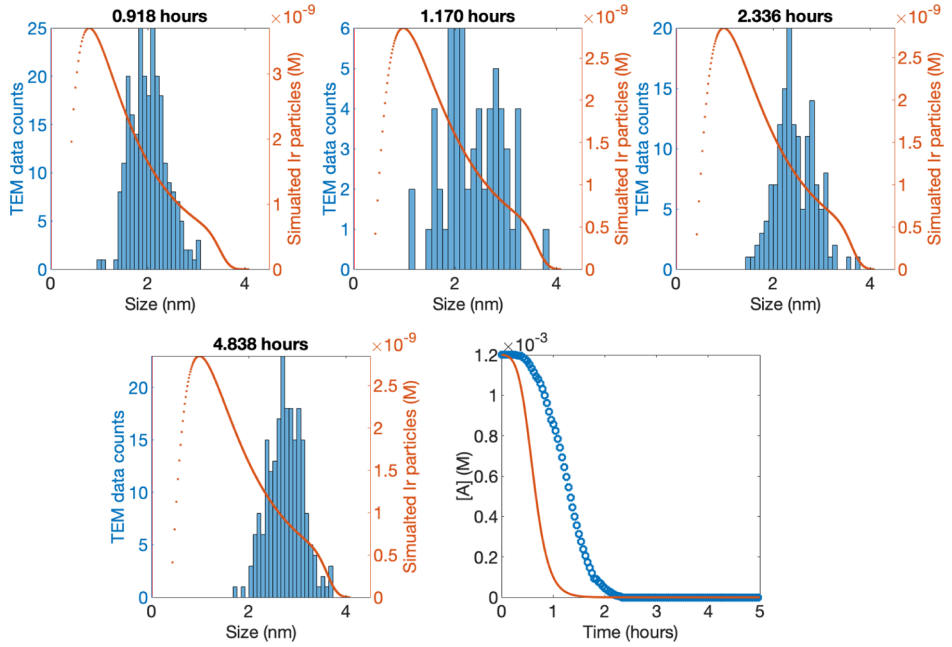

Figure 6. Fitting of the 4.838 h (fourth) histogram using the two-step ME-PBM with third-order nucleation and then simulation of the earlier histograms from the parameters of that fourth histogram fit. The resulting rate constants are $k_1 = 2.46 \times 10^3$ M^{-2} h^{-1}, $k_2 = 1.18 \times 10^4$ M^{-1} h^{-1}. BFV value of 3.87×10^2.

determined nucleation mechanism and the validity of the concept of requiring that experimentally known nucleation mechanism in the PBM—that is, the concept of mechanism-enabled PBModeling.

4.2. Four-Step ME-PBM. The results using the four-step, termolecular nucleation, mechanism-enabled PBModel in eq 8 are presented in Figures 8 and 9. In Figure 8, we see the results of fitting, to start, to the CHCRR kinetics curve. The four-step ME-PBM has no problem reproducing the sigmoidal CHCRR. But, similar to the two-step PBM, the four-step ME-PBM then produces simulated particle-size distributions that do not match the TEM PSD data.

Figure 9 shows the result of attempting to match the fourth TEM-determined PSD. In comparison to the two-step ME-PBM

https://dx.doi.org/10.1021/acs.jpcc.9b11239
J. Phys. Chem. C 2020, 124, 4852−4880

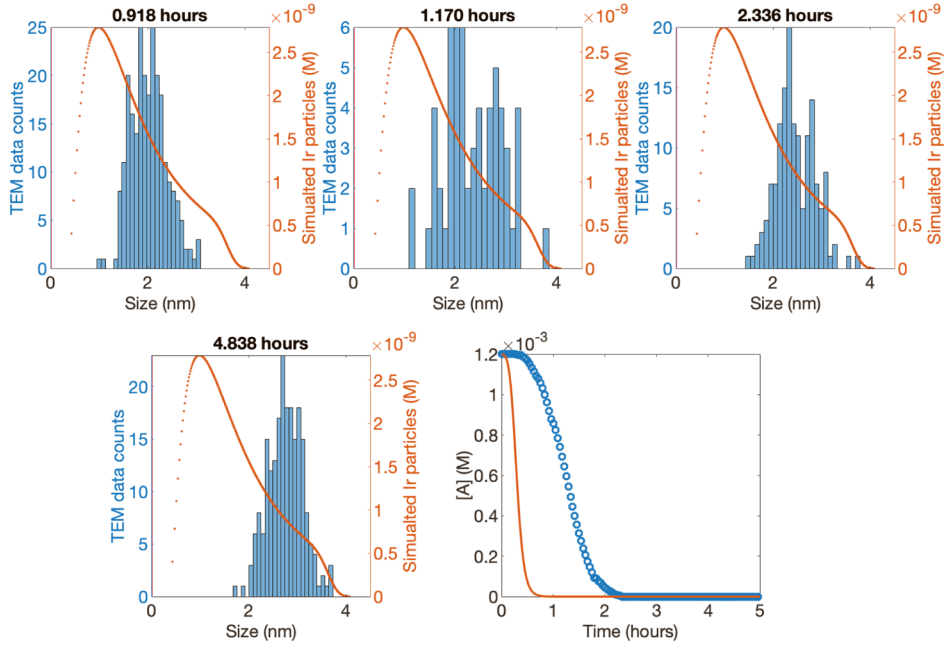

Figure 7. Results from simultaneous fitting of all four histograms using fminsearch and the two-step ME-PBM with third-order nucleation. The rate constants obtained after fitting are $k_1 = 5.11 \times 10^3\ M^{-2}\ h^{-1}$, $k_2 = 2.50 \times 10^4\ M^{-1}\ h^{-1}$ which were used to generate (a) the histograms, and (b) a (very poorly matching) CHCRR curve. BFV of 1.34×10^3.

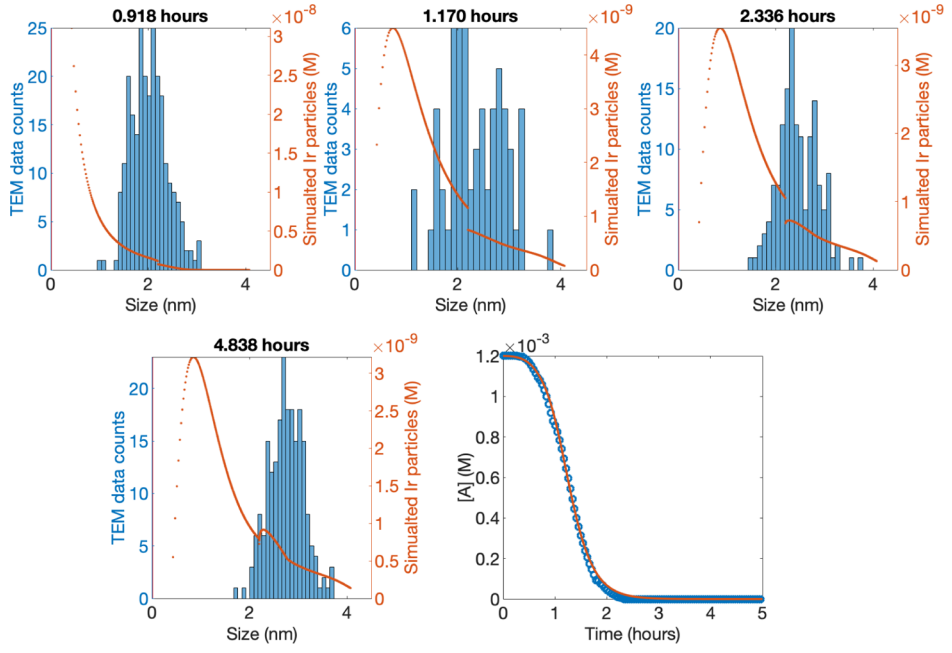

Figure 8. Results from fitting the four-step ME-PBM to the CHCRR curve to the right yielding: $k_1 = 1.06 \times 10^3\ M^{-2}\ h^{-1}$, $k_2 = 5.61 \times 10^3\ M^{-1}\ h^{-1}$, $k_3 = 16\ M^{-1}\ h^{-1}$, $k_4 = 8.69 \times 10^3\ M^{-1}\ h^{-1}$, and a B vs C ("small" vs "large") particle size cut-off of $M = 394$. The use of these k values to simulate the four PSDs provides a poor accounting of the PSD data. BFV of 1.45×10^{-4}.

results shown back in Figures 5−7, use of the four-step ME-PBModel with termolecular nucleation does show that a decent fit to at least one of the PSD histograms is possible. The fits yield $k_2 \gg k_4$; that is, smaller particles need to grow faster than larger ones in order to fit the data,[7] a critical result that will prove to be more general in the additional ME-PBModeling and fits that follow. However, a compelling, quantitative accounting of the PSD data is clearly not possible using the four-step ME-PBModel. Hence, additional ME-PBMs were investigated.

4.3. New Three-Step ME-PBM. Recall that the new, three-step mechanism, still containing termolecular nucleation, grew out of the finding that curve fits with the k_3 agglomeration step yielded $k_3 \approx 0$. This finding in turn lead to the hypothesis of adding the A + B → 2B, and B + B → C steps of the four-step mechanism to yield a composite A + B → C step as part of a new, minimalistic three-step mechanism and ME-PBM perhaps able to fit the CHCRR and PSD data. As Figure 10 shows, the new three-step ME-PBModel is able to fit the CHCRR kinetics curve to the bottom right in Figure 10. However, as in the previous

https://dx.doi.org/10.1021/acs.jpcc.9b11239
J. Phys. Chem. C 2020, 124, 4852−4880

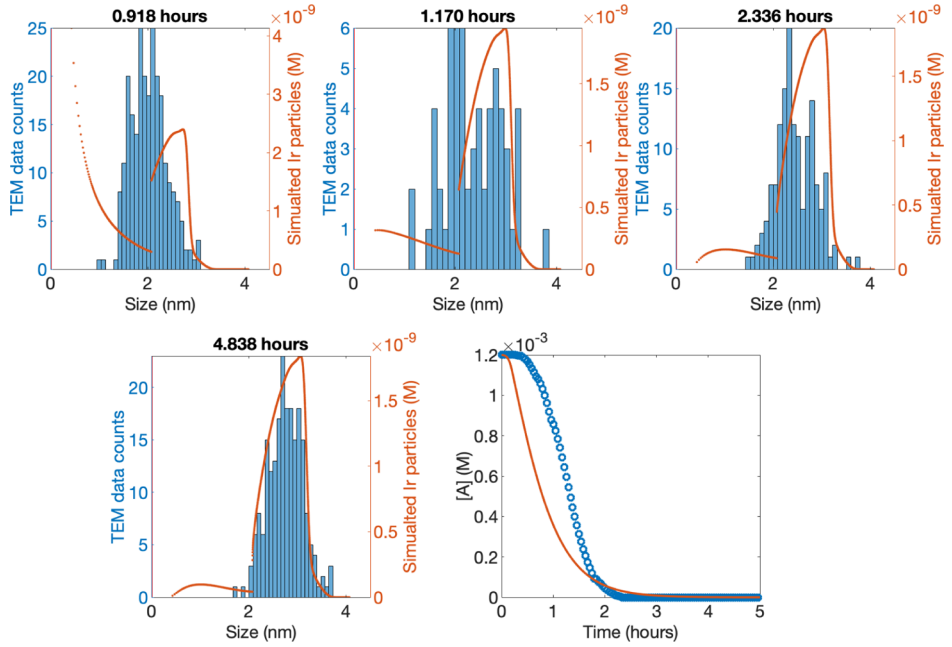

Figure 9. Results from fitting the four-step ME-PBM to the fourth PSD histogram giving the constants: $k_1 = 2.71 \times 10^3\ M^{-2}\ h^{-1}$, $k_2 = 2.00 \times 10^4\ M^{-1}\ h^{-1}$, $k_3 = 936\ M^{-1}\ h^{-1}$, $k_4 = 3.94 \times 10^3\ M^{-1}\ h^{-1}$, and B vs C cut-off of $M = 331$. While the PSDs are beginning to be better fit, the simulated CHCRR to the right and from the k values of the PSD fit is poor, even in the initial section where the CHCRR kinetics data are most reliable. The BFV is 4.62×10^1.

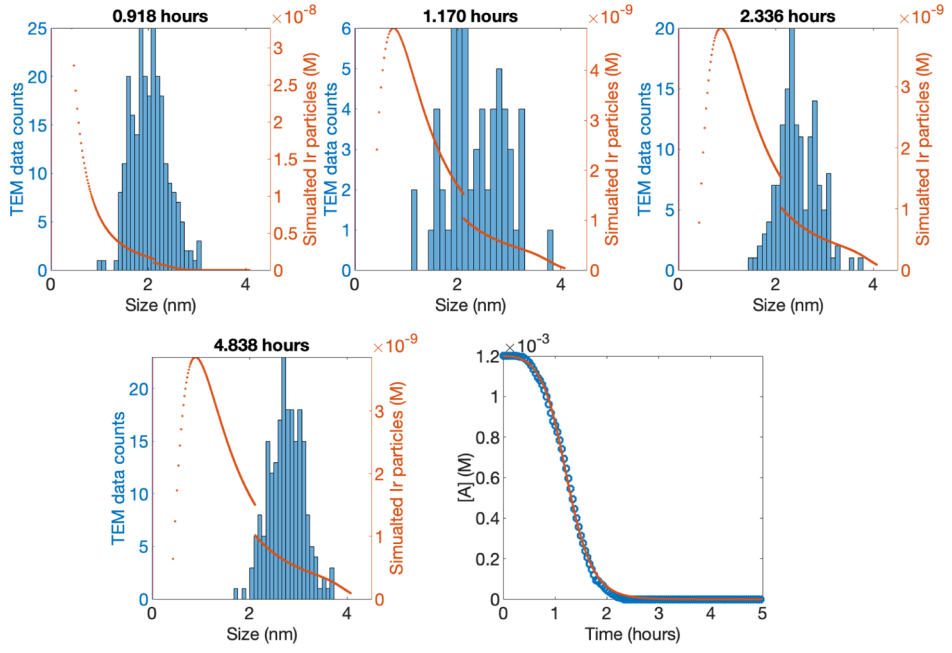

Figure 10. Fit to the CHCRR curve using the new three-step ME-PBM and then use of those rate constants to try to fit the PSDs to the left. The resulting rate constants are $k_1 = 1.13 \times 10^3\ M^{-2}\ h^{-1}$, $k_2 = 5.58 \times 10^3\ M^{-1}\ h^{-1}$, and $k_3 = 8.24 \times 10^3\ M^{-1}\ h^{-1}$, and B vs C cutoff of $M = 350$. BFV of 1.25×10^{-4}.

models and their fits, the rate constants which result from fitting the CHCRR do not permit a simultaneous, satisfactory fit to the information-laden particle-size distributions.

To determine if the new three-step ME-PBModel can fit the PSDs, we once again fit to the fourth time PSD data with the results in Figure 11. The fit to the fourth histogram is good. The simulated distributions for the three earlier time PSD histograms are generally good, but have peaks in especially the shorter time PSDs that are shifted a bit too far to the right compared to the experimental data. The fit to the CHCRR is again poor.

The new three-step ME-PBM is able to reproduce the experimental PSDs reasonably well. The fits in comparison to those of the four-step ME-PBM provide solid evidence that agglomeration per se is not essential to reproduce the PSD. Getting the shape correct for the fourth PSD and where the fit was done is an important result in its own right, one only possible with our full ODE approach to the population balance. Noteworthy in the three-step fit is that, once again, $k_2 > k_3$ is observed, by about ~6-fold in this particular ME-PBM. This "smaller particles grow more quickly than larger particles"

https://dx.doi.org/10.1021/acs.jpcc.9b11239
J. Phys. Chem. C 2020, 124, 4852−4880

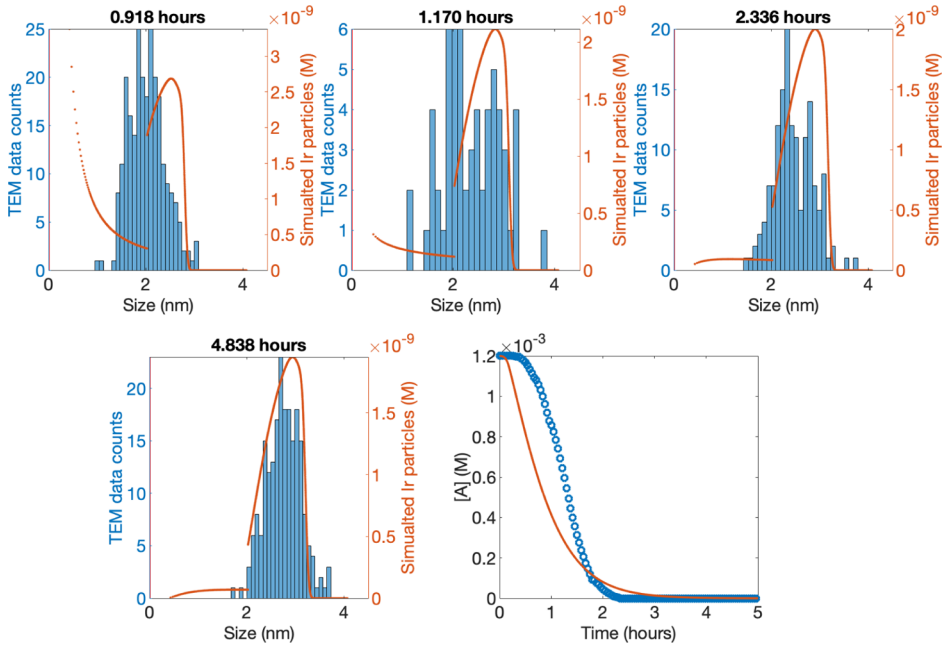

Figure 11. Fit of the fourth histogram using the new three-step ME-PBM. The rate constants are $k_1 = 1.95 \times 10^3\ M^{-2}\ h^{-1}$, $k_2 = 2.24 \times 10^4\ M^{-1}\ h^{-1}$, and $k_3 = 3.63 \times 10^3\ M^{-1}\ h^{-1}$, and B vs C cut-off of $M = 308$. The simulation of the CHCRR shown is, as in earlier figures, using these constants from the fourth PSD fit. BFV of 44.3.

finding is a key insight seen throughout this and the other mechanisms tested.

The discovery of the new three-step mechanism is another important finding from the present work. This is an example of the power of ME-PBM in approaching the typically much more challenging "inverse problem" in science, in the present example the problem of going from the PSD data (the "effects") back to the most plausible and best-supported mechanism (the "cause"). Restated, ME-PBM is shown by this example to be an effective tool not only with the "forward problem" of connecting rigorously obtained, minimalistic, disproof-based mechanisms to their PSDs but very importantly also in the reverse, "inverse problem" of refining the minimal mechanism best able to account for the data.

Summarizing briefly the results to this point, the two-step ME-PBM fails to provide a fit to the PSD, the four-step succeeds, but has an extra B + B → C agglomeration step that the fitting shows is unnecessary. The new three-step mechanism with termolecular nucleation and its associated ME-PBM fits the PSD reasonably well. Moreover, comparing the three-step to the two-step ME-PBModel yields a valuable physical insight: in terms of its growth kernel, the three-step ME-PBM differs from the two-step ME-PBM only by replacing the constant, single growth rate constant (k_2 in the two-step ME-PBM) by a two-step growth function, one that allows a decreasing growth with increasing particle size (modeled in the three-step ME-PBM by a step-function $k_2 > k_3$). The critical insight here is that the large particles must grow more slowly compared to the small particles to give the observed, relatively narrow PSDs.

Put another way, nucleation and growth need NOT be completely separated in time, for example, by putative "burst" nucleation, as the widely cited LaMer[5,69] model of particle formation assumes. Instead, nucleation can be and probably often is continuous, as first shown in 1997.[6] Near-monodispersity in size can be achieved by the smaller particles growing more quickly so that they "catch up" in size to the more slowly growing, larger particles.[7] This is a huge, paradigm-shifting mechanistic insight in the understanding of how narrow particle sizes can form.

Additionally, analysis of the information-laden PSD via PBM is able to inform and refine the mechanism, a proof-of-principle of addressing the challenging inverse problem here in going back from the PSD to test and refine as needed the postulated mechanism of particle formation.

4.4. Two-Step, Alternative Termolecular Nucleation PBM. A fit to the CHCRR can be seen in Figure 12 and a fit to the final PSD histogram (i.e., at the end time of 4.838 h) using this ME-PBM can be seen in Figure 13. In Figures 12 and 13 (and all subsequent fits where the experimentally determined alternative termolecular nucleation mechanism will be part of the ME-PBM), the $K_{Diss} = k_{+Diss}/k_{-Diss}$ was constrained to its experimental value in acetone[70] of $K_{Diss} = 4.95 \times 10^{-7}\ M^{-1}$ at 22 °C, implemented via the ratio of $k_{+Diss} = 3.60 \times 10^{-2}\ M^{-2}\ h^{-1}$/ $k_{-Diss} = 7.27 \times 10^4\ M^{-1}\ h^{-1} = K_{Diss}\ (M^{-1})$. Additionally, the experimentally known constraint was added of using $k_{1alt} = (6.4 \pm 1.6) \times 10^4\ M^{-2}\ h^{-1}$ and the indicated error bars as upper (i.e., $8.0 \times 10^4\ M^{-2}\ h^{-1}$) and lower (i.e., $4.8 \times 10^4\ M^{-2}\ h^{-1}$) constraints to the curve-fitting. This ability to input not only the experimentally determined nucleation mechanism but also the experimentally determined K_{Diss} value and k_{1alt} values is another important component of this specific mechanism-enabled PBM—and a desirable component of any ME-PBM, that is, using all available experimental information as input to the ME-PBM. In the present case, that input means that the result the PSD curve-fitting is, then, a much more rigorous test of the ME-PBM being examined as it has two less parameters (and in the two-step mechanism, only three adjustable parameters, k_1 and k_2 and M, the small vs large particle cutoff value), with which to try to fit the whole PSD, including its shape.

The attempted fits to the two-step alternative termolecular nucleation ME-PBM to either the CHCRR or the final histogram are unable to produce a narrow enough size

https://dx.doi.org/10.1021/acs.jpcc.9b11239
J. Phys. Chem. C 2020, 124, 4852−4880

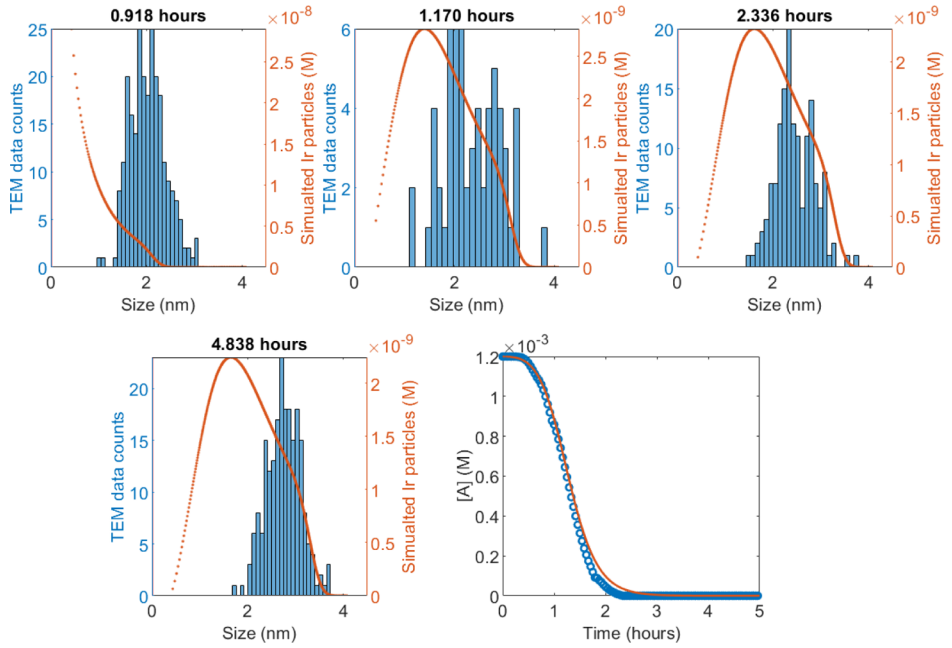

Figure 12. Results from attempted fitting of the two-step, alternative termolecular nucleation ME-PBM to the CHCRR to start. The rate constants $k_{+Diss} = 3.60 \times 10^{-2}$ M^{-2} h^{-1}, $k_{-Diss} = 7.27 \times 10^{4}$ M^{-1} h^{-1} were fixed in this and all subsequent PBMs that contain the alternative termolecular nucleation mechanism. The resultant rate constants from the fit are $k_{1alt} = 4.80 \times 10^{4}$ M^{-2} h^{-1}, $k_2 = 6.50 \times 10^{3}$ M^{-1} h^{-1}. BFV of 1.04×10^{-3}.

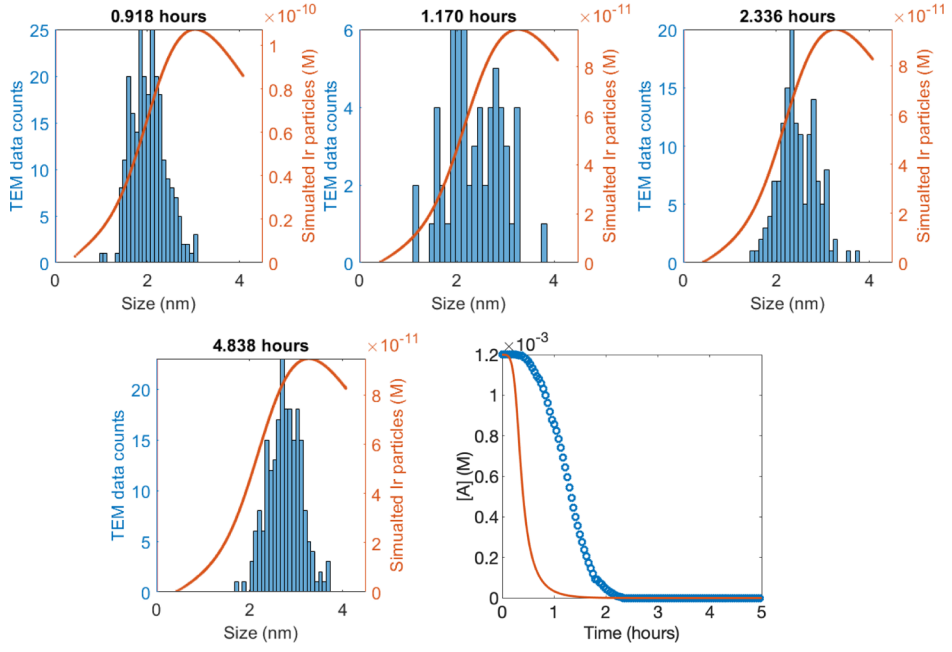

Figure 13. Results from fitting of the final, 4.838 h histogram using the two-step alternative termolecular nucleation ME-PBM. The resultant rate constants from the fit are $k_{1alt} = 4.80 \times 10^{4}$ M^{-2} h^{-1}, $k_2 = 3.99 \times 10^{4}$ M^{-1} h^{-1}. BFV of 253.

distribution; the fit to the PSD histogram accounts at most for just part of the leading edge of the histogram. The CHCRR fit in Figure 12 matches fairly well; however, the associated PSDs are both too wide and have means which are too small. The final histogram fit in Figure 13 also suffers from PSDs which are too wide but now additionally has means which are too large. Its associated CHCRR curve is a poor match to the experimental values.

In short, the simple two-step model is again unable to account for the PSD, even when mechanistically enabled with the experimentally determined, alternative termolecular nucleation mechanism and the experimentally determined K_{Diss} and k_{1alt} as known, constrained input parameters.

4.5. Four-Step, Alternative Termolecular Nucleation PBM. A fit to the CHCRR curve to four-step mechanism was performed by using this ME-PBM, constraining K_{Diss} to its known, experimentally determined, value and using the experimental k_{1alt} and its error limits as upper and lower constraints on the fitting. As shown in the lower right of Figure 14, the fit to at least the CHCRR curve is not way off but does yield a slightly too long induction period. This slightly too long induction time is compensated for in the fit parameters, with a k_4

https://dx.doi.org/10.1021/acs.jpcc.9b11239
J. Phys. Chem. C 2020, 124, 4852−4880

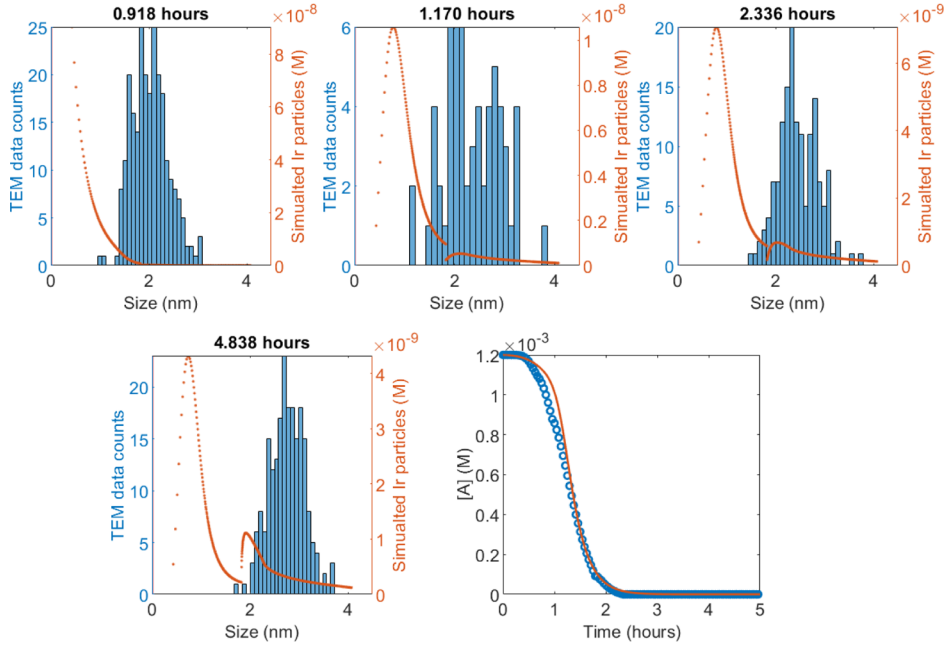

Figure 14. Results from fitting with the four-step, alternative termolecular nucleation ME-PBM to the CHCRR, shown to the right. The resulting rate constants from the fit are $k_{1alt} = 5.99 \times 10^4\ M^{-2}\ h^{-1}$, $k_2 = 4.21 \times 10^3\ M^{-1}\ h^{-1}$, $k_3 = 6.24 \times 10^2\ M^{-1}\ h^{-1}$, $k_4 = 1.68 \times 10^4\ M^{-1}\ h^{-1}$, and the B vs C particle size cutoff, $M = 225$. The associated histogram computed using these constants is shown as before on the left. BFV of 9.55×10^{-4}.

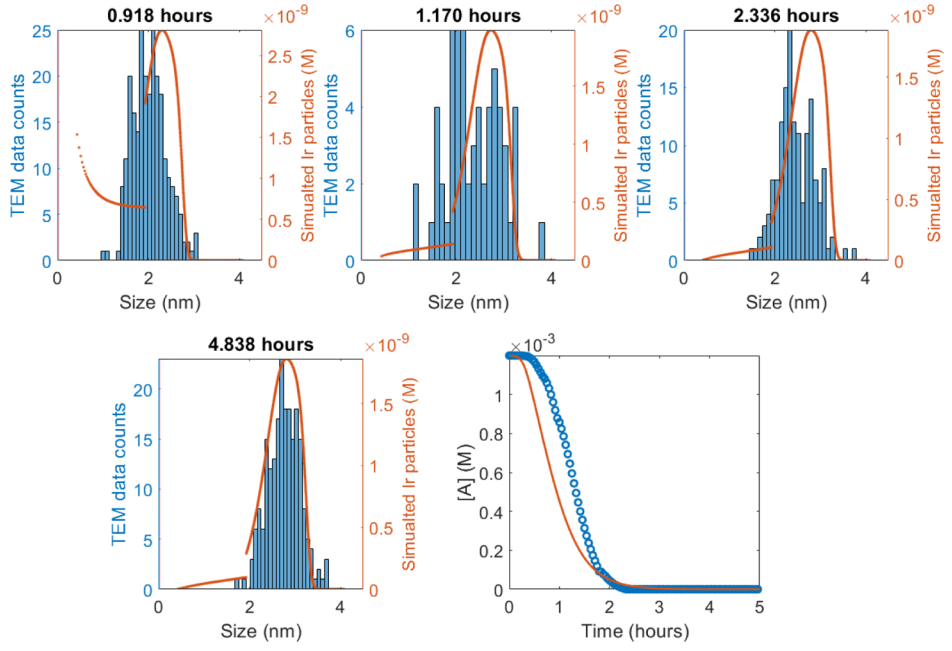

Figure 15. Fitting with the four-step, alternative termolecular nucleation ME-PBM to the fourth histogram obtained at 4.838 h. For fixed $k_{+Diss} = 3.60 \times 10^{-2}\ M^{-2}\ h^{-1}$, $k_{-Diss} = 7.27 \times 10^4\ M^{-1}\ h^{-1}$ values the patternsearch fit gives $k_{1alt} = 6.40 \times 10^4\ M^{-2}\ h^{-1}$, $k_2 = 1.61 \times 10^4\ M^{-1}\ h^{-1}$, $k_3 = 12\ M^{-1}\ h^{-1}$, $k_4 = 5.45 \times 10^3\ M^{-1}\ h^{-1}$, with $M = 265$. The associated CHCRR curve computed from using these rate constants is shown on the bottom right and has a similar slope, but shorter induction period. The BFV is 2.96×10^1.

that is significantly larger than k_2. The corresponding simulated PSD using the CHCRR-obtained rate constants starts as monotonic but ends bimodal, far different than the experimental PSDs. This PBModeling example teaches that quicker growth of large particles compared to growth of small particles does not yield an experimentally accurate PSD—indeed, is opposite of what is required for the observed, relatively narrow PSD.

Figure 15 results from using the four-step, alternative termolecular nucleation ME-PBM to fit to the fourth PSD histogram experimentally collected at 4.838 h. This, now most complex ME-PBM among those examined in detail, does an excellent job of matching the next-to-last, and final distributions, as well as a reasonable job of fitting the two earlier time histograms obtained at 1.170 and 2.336 h. However, the associated, simulated CHCRR curve, using the fourth PSD-obtained rate constants undercuts the reporter reaction data somewhat, Figure 15 bottom rightmost figure.

https://dx.doi.org/10.1021/acs.jpcc.9b11239
J. Phys. Chem. C 2020, 124, 4852−4880

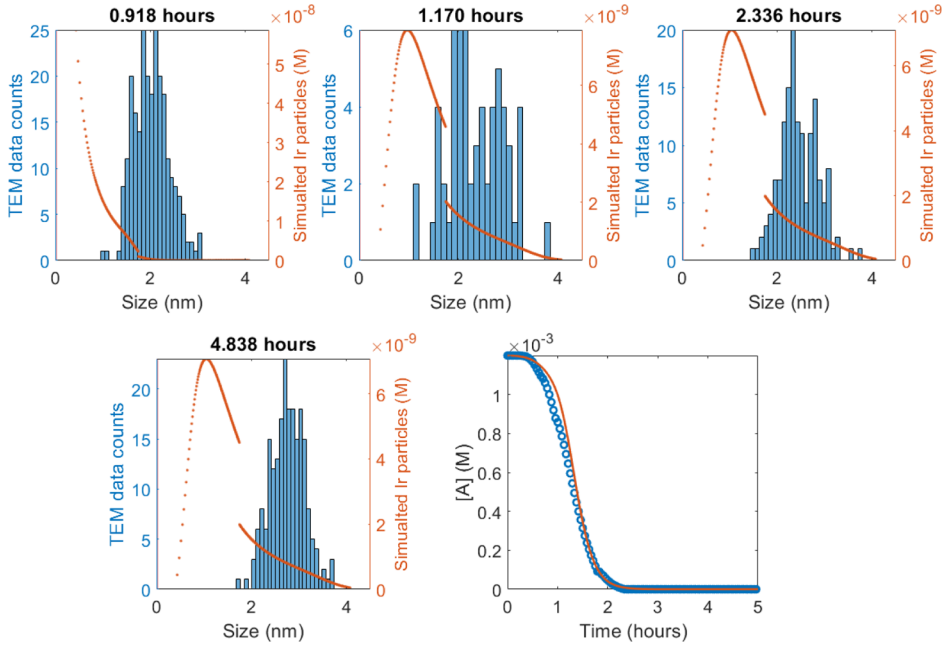

Figure 16. Fit of the CHCRR in the lower right using the new three-step, alternative termolecular nucleation ME-PBM, while constraining $k_{+\mathrm{Diss}} = 3.60 \times 10^{-2}\ \mathrm{M}^{-2}\ \mathrm{h}^{-1}$, $k_{-\mathrm{Diss}} = 7.27 \times 10^{4}\ \mathrm{M}^{-1}\ \mathrm{h}^{-1}$. The resulting parameters are $k_{1\mathrm{alt}} = 4.97 \times 10^{4}\ \mathrm{M}^{-2}\ \mathrm{h}^{-1}$, $k_2 = 4.97 \times 10^{3}\ \mathrm{M}^{-1}\ \mathrm{h}^{-1}$, and $k_3 = 1.12 \times 10^{4}\ \mathrm{M}^{-1}\ \mathrm{h}^{-1}$, and B vs C particle size cut-off, $M = 196$, which were in turn used to generate the simulations shown for the four histograms. BFV is 9.54×10^{-4}.

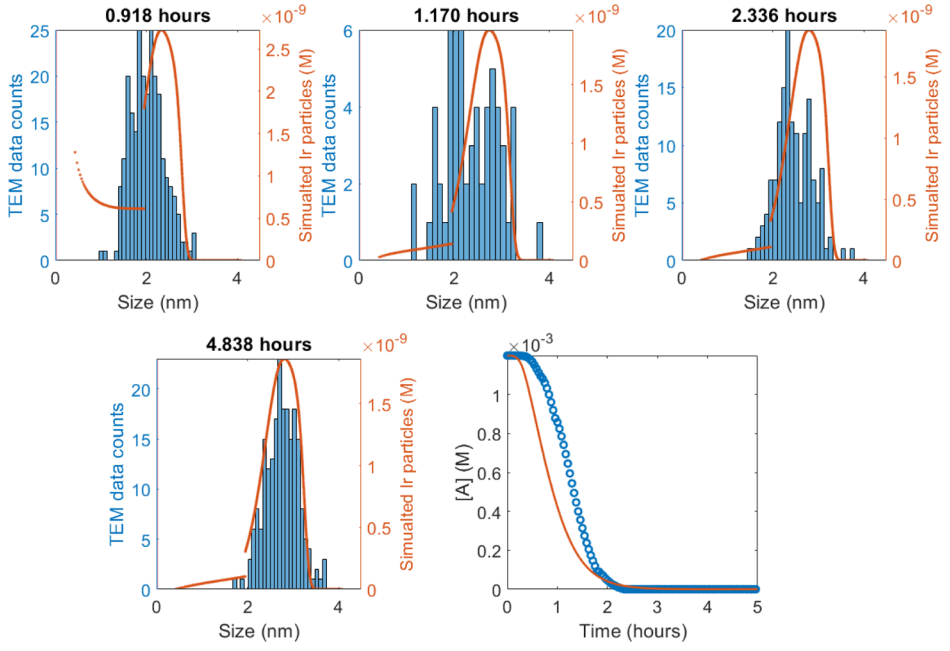

Figure 17. Fit of the final, 4.838 h histogram using the three-step, alternative termolecular nucleation ME-PBM, enabled by the experimentally established constraints $k_{+\mathrm{Diss}} = 3.60 \times 10^{-2}\ \mathrm{M}^{-2}\ \mathrm{h}^{-1}$, $k_{-\mathrm{Diss}} = 7.27 \times 10^{4}\ \mathrm{M}^{-1}\ \mathrm{h}^{-1}$. The resultant fit-determined rate constants are $k_{1\mathrm{alt}} = 6.55 \times 10^{4}\ \mathrm{M}^{-2}\ \mathrm{h}^{-1}$, $k_2 = 1.65 \times 10^{4}\ \mathrm{M}^{-1}\ \mathrm{h}^{-1}$, and $k_3 = 5.63 \times 10^{3}\ \mathrm{M}^{-1}\ \mathrm{h}^{-1}$, and B vs C particle-size cut-off, $M = 274$. The computed CHCRR curve using these parameters is shown to the right. The computed histograms for the first three, earlier time histograms are shown to the left. The BFV is 2.92×10^{1}.

Overall, the results from this to-date most complex ME-PBM, which includes the correct alternative termolecular nucleation mechanism and constrains $k_{1\mathrm{alt}}$ and K_{Diss} to their experimental values, demonstrate the following: (i) using this model and full ODE implementation employed here, we are able to FIT the PSD's general shape; (ii) the ME-PBModeling is able to distinguish mechanisms via their PBM-predicted PSDs; (iii) we have rather high-level PBModeling at this stage via our full ODE implementation with the ability to account reasonably well for the PSD evolution at the indicated times.

Additionally, (v) the success of this PBM is not an accident. Instead, that success comes from the mechanism-enabled PBModeling, including the knowledge and hence input of the experimental nucleation mechanism as well as the experimental K_{Diss} value and the experimental limits on $k_{1\mathrm{alt}}$. (vi) The ME-PBModeling in turn provides further, quantitative support for the correctness of alternative-termolecular nucleation in the

https://dx.doi.org/10.1021/acs.jpcc.9b11239
J. Phys. Chem. C 2020, 124, 4852−4880

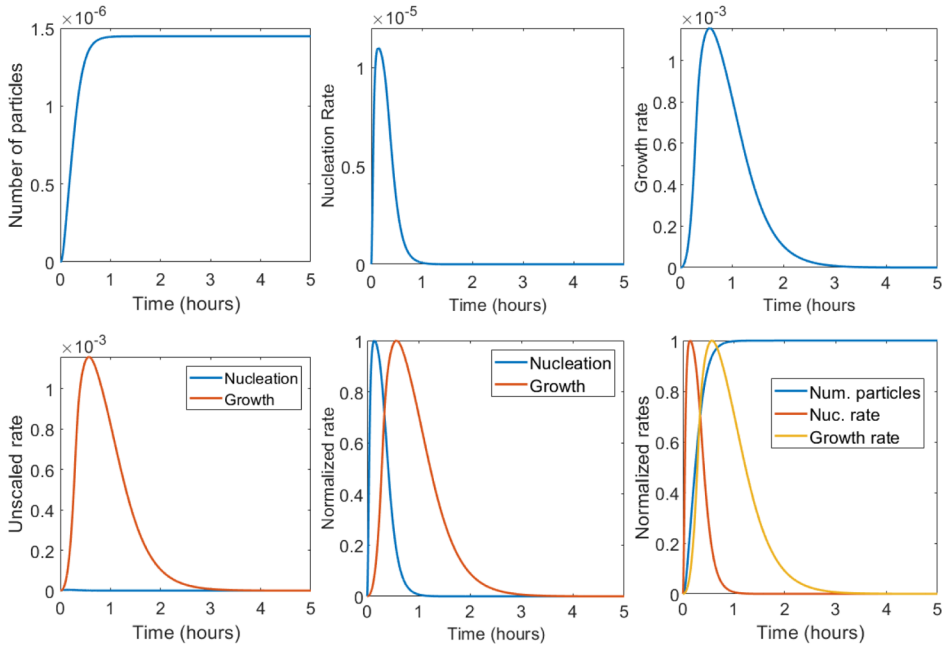

Figure 18. Numerically calculated number of particles (M), nucleation rate (M h^{-1}), and growth rate (M h^{-1}) for the three-step mechanism with alternative termolecular nucleation. Both unscaled and scaled versions of the nucleation- and growth-rate curves are shown as the bottom figures; note that the unscaled nucleation and growth rates in the bottom left figure show the dominance as expected of growth in consuming the precursor, A. The number of particles increases monotonically demonstrating the continuous nucleation of particles. The nucleation rate spikes and appears burst-like but results from continuous nucleation. The spike periods of nucleation and growth where the two rates are both relatively very high overlap for approximately one-fifth of the measured time.

present case—all of our simulations were improved, at least somewhat, when using the experimentally derived, alternative-termolecular nucleation step as part of the ME-PBModel, even when compared to the postulate of simple termolecular nucleation (although a caveat here is that the four-step model with alternative-termolecular nucleation has the largest number of adjustable parameters (6 total) of any ME-PBM examined in the main text). A final important point apparent from all of the PBModeling to this point is that (vii) our results teach that fitting the PSD including its shape is not easy nor trivial; instead, fitting the information-rich PSD shape looks to be a stringent test of the proposed, enabling mechanism, one possible with the full ODE implementation approach developed and employed herein.

4.6. New Three-Step Mechanism, Alternative Termolecular Nucleation PBM. When this final ME-PBM was used to fit the CHCRR reaction, it suffered the same issue as the two- and four-step mechanisms as shown in Figure 16, even when including the experimentally determined nucleation mechanism, namely, that the associated PSDs are poorly fit using the rate constants from the CHCRR fit; the simulations to the PSDs have too many small particles, not that these simulations use an updated, one-line-corrected version of the coded ODEs previous used[7] as detailed in the Experimental Section. (As noted earlier, the original version of the code had the POM mass balance equation only use k_2 instead of k_2 and k_3; both the original and updated code can be found at https://github.com/drhandwerk/pbm). The effect on the fitted rate constants is minor, being only in the second decimal point.

However, when we fit the final, 4.838 h PSD histogram (rather than the CHCRR), this final model produced the most accurate size-distribution fit among the 12 total models tested. As seen in Figure 17, not only does the simulation match well including the PSD shape in the 4.838 h histogram but also the earlier three PSDs are fairly well-matched—this model being the only simulation that resulted in a reasonable fit to the first, early-time PSD histogram. Noteworthy in this context is that fitting the final, 4.838 h histogram using the standard three-step and four-step ME-PBMs, enabled with simple termolecular nucleation, produced the next-best early time distributions. However, those two earlier models still have the problem of producing too many small particles. The simulated CHCRR curve, based on the rate constants obtained from fitting the final, 4.838 h histogram, has the correct general shape and curvature, but is not yet an excellent match of the experimental CHCRR as it undercuts the experimental curve. The reasons for the discrepancy are under further investigation, although we again note that the assumptions and approximations underlying the CHCRR are known to fail once the cyclohexene and H_2 decrease in the latter half of the CHCRR curve.[4,6,18−22]

A main physical finding from our PBM efforts is that in order to arrive at a correct shape distribution the larger particles must grow more slowly than the smaller particles; that is, $k_2 > k_3$. For the four- and three-step mechanisms that have size-dependent monomer growth rates, the rate constants for the larger particles are always smaller than the rate constants for the smaller particles, see, for example, k_2 and k_4 in Figure 16 or k_2 and k_3 in Figure 17.

Of considerable significance here is that our results are also consistent with and fully supportive of the 2019 findings of Karim and his group who studied a cleverly chosen Pd/ligand nanoparticle system at higher temperatures by small-angle X-ray scattering (SAXS), density functional theory calculations, and PBM using the MoM.[55] Highly relevant to the present study is that their PBM is mechanistically enabled by the two-step mechanism in Scheme 1 plus an A·L ⇌ A + L prior equilibrium (analogous to the K_{Diss} in the alternative termolecular mechanism[23]). Additionally relevant is their very important

https://dx.doi.org/10.1021/acs.jpcc.9b11239
J. Phys. Chem. C 2020, 124, 4852−4880

recent finding of a ligand-capping, pseudo-elementary step-based, B + L ⇌ B·L equilibrium.[54] A primary conclusion of their recent work is, pleasingly, precisely the same finding as given above that (quoting their Abstract) "...larger nanoparticles grow slower than smaller ones", but now in their Pd_n system with $POctyl_3$ ligands.[55] That important work additionally provides good evidence that nanoparticle surface ligation, and apparently lower ligand coverage in the smaller particles,[55] is responsible for the size focusing seen throughout the reaction and despite continuous nucleation as first discovered and precedented in 1997 via the two-step mechanism[6] in Scheme 1. Collaborative studies with the Karim group are in progress aimed at a number of important objectives raised by their and the present studies. One study in progress is a comparison of the two different, minimum mechanisms supported by the present (Ir) and the (Pd) studies. A second study also in progress is a comparison of the present full-ODE and the MoMs approaches to PBModeling.

Further support for the concept of mechanism-enabled PBM that is the central theme of the present contribution comes from a look at the one prior attempt to use PBM (via the MoMs) with the two-step mechanism.[52] That study, which was not correctly mechanistically enabled by knowledge of the critical (alternative termolecular) nucleation mechanism, but, instead tried to use inapplicable[4,5,23] CNT, reached the erroneous conclusion (for the identical Ir(0) nanoparticle system studied herein and the same $Ir(0)_n$ formation data) that there must be a "...delayed onset of nucleation and its suppression soon after..."[52] in order to fit the observed PSD data. That conclusion is incorrect as we noted previously that it would probably be (see footnotes 72 and 75 elsewhere[4]): both the present work, and that from the Karim group,[55] disprove the prior, erroneous conclusion that there must be a delayed onset of nucleation and its suppression soon after. Given that the above incorrect conclusion (that continuous nucleation must somehow be stopped) was reached by an expert in PBM trained in the labs of a premier practitioner of PBM, the important insight here is clear: only true, rigorous mechanism-enabling of ones PBM, plus a highly disproof-based scientific method as part of the PBModeling, holds hope of leading one to correct, reliable PBM-derived conclusions.

5. NUMBER OF PARTICLES AND NUCLEATION AND GROWTH RATES FOR THE NEW THREE-STEP MECHANISM ENABLED WITH ALTERNATIVE-TERMOLECULAR NUCLEATION

The number of particles, nucleation rate, and growth rate were calculated for the simulation appearing in Figure 17. The nucleation rate is $3k_{1alt}n_1n_s^2$ (see the Supporting Information under eq S11 for details) and the growth rate is $k_g n_1 \sum_{i=3}^{\infty} r(i) i n_i$; note that these are written as they should be as their positive values. Care is required in accounting for the statistical factors involved for the number of n_1 involved in a given step as discussed in more detail directly under eq S11 of the Supporting Information. The nucleation and growth rates from this ME-PBM are shown in Figure 18.

The curve for the number of particles increases rapidly and appears to plateau but actually is monotonically increasing through the reaction—as expected for the continuous nucleation that is part of the ME-PBModel. The nucleation and growth rates have windows of relatively high values. The nucleation rate spike lasts for approximately an hour and its decrease is inverse of the growth rate's increase—clearly showing their coupling as apparent in the three-step mechanism and its associated kinetics differential eq S11. The growth rate begins to increase immediately, increases rapidly, and then decays as precursor is consumed. The growth phase overlaps with the nucleation phase and they are never separated completely in time.

Of considerable interest and worth noting is that the nucleation rate spike in the top middle figure looks like a prime example of what many researchers would have labeled (at least before[5]) as supporting the LaMer model of "burst nucleation". Actually and instead, that spike results from continuous nucleation[6] that is net termolecular in[23] Ir, with Ir_3 as the kinetically effective nucleus.[4]

6. CONCLUSIONS

The following are the primary conclusions resulting from our ME-PBM studies and the full details made available by the present contribution. A main goal of the present paper is to equip with ME-PBM anyone who is interested in its use for their own particle-formation reaction and associated kinetics and mechanistic analyses.

- The concept of mechanism-enabled PBModeling has been introduced by our prior[7] and the present study, specifically the notion of enabling one's PBM, regardless of where it occurs across nature, with experimentally determined, hence more reliable mechanisms for particle formation and subsequent reactions. Those rigorously obtained mechanisms are by definition disproof-based, Ockham's razor-obeying, therefore deliberately and necessarily minimalistic, pseudo-elementary step-based, experimentally determined mechanisms. The evidence herein suggests that such mechanism-enabled PBM is an important advance in both how PBM needs to be done, and then in the success one can expect from the resulting ME-PBM.
- The PBModeling fully supports the use of the pseudo-elementary step approach for determining the minimum mechanisms used to initially fit and interpret experimental particle formation kinetic data,[4,18−24,26] and then their use to enable the ME-PBM. Specifically, the ME-PBM shows that even atomistic models with 2500 elementary steps can be readily built and successfully used based on experimentally obtained, disproof-based, two- to three-pseudo-elementary-step mechanisms. The pseudo-elementary step concept[6,53] is further supported as an important concept in dealing with complex chemical reaction dynamic systems.
- The importance of employing a disproof-based approach in one's PBModeling was also both emphasized and successfully employed.
- A series of twelve total mechanisms was considered. The six mechanisms that provided the closest fits to the experimental PSDs were presented. The experimentally determined alternative termolecular nucleation proved to be the best fitting ME-PBM from among the 12 mechanisms examined, a model that has 6 parameters (5 rate constants and the M value), but where the number of adjustable parameters was reduced to 4 in the fitting by the experimentally known K_{Diss} and k_{1alt} constraints.
- The PBModeling was implemented via a full ODE approach, an approach little used since its 1918 origins,[63,64] but a powerful approach that allows direct

https://dx.doi.org/10.1021/acs.jpcc.9b11239
J. Phys. Chem. C 2020, 124, 4852−4880

computation of the PSD including its shape. The full ODE approach also allows curve-fitting of the experimental PSD to a postulated ME-PBM.

- Nearly all of the ME-PBModels examined were able to reproduce the sigmoidal CHCRR curve that indirectly monitors the loss of precursor A, revealing the important insight that a fit to just that particular kinetics curve is, by itself, an insufficient test en route to the true underlying mechanism, an important insight with additional implications.[71] The simplest, classic, deliberately minimalistic FW two-step mechanism[6] is unable to reproduce the observed PSD regardless of the precise nucleation mechanism used to expand it—although a simple 1-step expansion of the two-step mechanism that allows for size-dependent growth is a critical part of the mechanism able to fit the PSDs.
- The needed, additional complexity that one must add to the classic two-step mechanism to be able to fit the PSD data is then: (i) the experimentally correct nucleation mechanism—continuous,[6] alternative-termolecular nucleation[23] and then (ii) an overall three-step mechanism in which there can be differential growth of "smaller" versus "larger" particles. That said, the two-step mechanism is expected to continue to be useful in cases where fitting of just the particle formation, raw kinetics data (i.e., and not any PSD data) is needed.
- The new three-step mechanism[7] resulted from the ME-PBM examining a four-step mechanism: the fitted rate constant for the B + B → C agglomeration step of the four-step ME-PBM tended toward $k_3 \approx 0$. This in turn implies, physically, that agglomeration is not kinetically important in the present $Ir(0)_n$ formation system and under the experimental conditions examined. This $k_3 \approx 0$ finding from the ME-PBM, and hence lack of kinetically detectable agglomeration, is consistent with and supportive of all of the prior curve-fitting and mechanistic work for the Ir(0) system[4,6,18−23] based primarily on the CHCRR methodology.[71] Adding the A + B → 2B and B + B → C steps to give a single, replacement A + B → C step yielded a new three-step minimum, pseudo-elementary step mechanism[6,53] based on the ME-PBModeling as the overall best performing ME-PBM.
- The resultant three-step ME-PBM teaches the physical insight that, post the correct nucleation, particle growth is fundamentally monomer addition, at least under conditions where agglomeration is not kinetically competitive. This yields the best evidence to date that the A + B → 2B autocatalytic pseudo-elementary step of the basic two-step mechanism represents the summation of the individual $A + B_j \rightarrow B_{j+1}$ monomer addition steps. This finding in turn reinforces the use of a full ODE approach to the PBM whenever possible, as the full ODE takes into account each of those possible monomer addition steps.
- The discovery of the new three-step mechanism[7] is an example of use of ME-PBM to inform the "inverse problem" by inducing mechanism ("cause") from observables ("effects"), that is, where one uses the PSD data and PBM to refine the proposed mechanism and to upgrade the starting ME-PBM.
- The additional complexity one needs to add beyond the classic FW two-step mechanism to capture the PSD is, however and of course, neither unexpected nor bad. Instead, that added mechanistic complexity is the normal, stepwise, evolutionary nature of mechanistic science as one attempts to provide a solution to the inverse problem. Postulated solutions to any inverse problem in science and nature must, as epistemology teaches, necessarily start from and build off of Ockham's razor-obeying, minimalistic explanations, in this case the 1997 FW two-step mechanism.[6] The ME-PBM does, however, fully support the mechanistic work leading to the original FW two-step minimum mechanism and its finding[6] that agglomeration is not needed to account for that CHCRR or, now, the PSD data, at least for the present $Ir(0)_n$ nanoparticle formation system examined.
- Critically, matching the ME-PBMs to the PSDs versus time proved to be a stringent test of the underlying minimum mechanisms, as expected because the information-rich PSD is intrinsically the physical composite of all of the kinetics information from all of the underlying steps occurring during the particle synthesis. Restated, our results strongly suggest that ME-PBM needs to be used henceforth to test any and all future, proposed particle-formation mechanisms.
- The evidence is now compelling that the FW two-step and the new HSW-FW three-step minimum mechanisms with their physical insight of continuous nucleation[6]—the opposite of the now disproven[5] LaMer model with its instantaneous-nucleation assumption[69]—are another major paradigm shift in the understanding of particle formation across a wide variety of systems in nature. The evidence for this includes the use of the FW two-step mechanism in over 560 literature citations at present to account of the kinetics of systems ranging from homogeneous catalyst formation,[56,72,73] heterogeneous catalyst formation,[74−76] protein aggregation,[77−80] solid-state kinetics,[81,82] dye aggregation,[83] and other areas of nature showing "cooperative", autocatalytic phenomena.[84] The FW two-step mechanism provides slow, continuous nucleation and autocatalytic surface growth. The bulk of the existing evidence is that these concepts should replace inapplicable CNT[4,5] (i.e., inapplicable to strong-bonding systems) as well as the often cited LaMer postulate of putative "instantaneous" nucleation and "diffusion-controlled" growth.[5] "Instantaneous/burst" nucleation has no compelling evidence that we can find, even in our recent comprehensive review examining the 1953 total papers (as of April 2019) that cite the LaMer model.[5,69] The reader probably noted that the fastest growth rate constant found herein is ca. $\leq 10^8$ slower than diffusion control—and, hence, chemical-reaction-rate controlled (and taking diffusion control as ca. 10^9 M^{-1} s^{-1}, which is ca. 4×10^{13} M^{-1} h^{-1} for comparison to the M^{-1} h^{-1} second-order, k_2 and k_3 growth rate constants herein).
- The nucleation rate versus time in Figure 18 exhibits a spike that, previously, many would probably have assigned to the LaMer model of putative instantaneous nucleation. However, the spike in the nucleation rate actually arises from continuous, alternative termolecular nucleation. That net Ir_3 at the nucleation rate-determining step just naturally has its highest rate soon after the reactants are mixed and when the Ir-precursor is at its highest, starting concentration. The take-home lesson is that one cannot just "eyeball" a peak in some concentration profile and

https://dx.doi.org/10.1021/acs.jpcc.9b11239
J. Phys. Chem. C 2020, 124, 4852−4880

then claim it supports, for example, the LaMer model of putative instantaneous nucleation.[5]

- The second key finding supported by all our PBM is the new physical insight that smaller particles must grow more quickly than larger ones,[7] differential growth that allows the smaller particles from continuous nucleation[6] to catch up in size with more slowly growing larger particles, leading in turn to near-monodisperse PSDs. This "smaller grow more quickly than larger particles" insight is a second, paradigm-shifting insight, one that replaces the need for the assumption of "instantaneous nucleation" in the LaMer model which has dominated thinking about how uniform particle might have been formed since 1950 and hence for the prior 69 years.[69]
- The $k_2 > k_3$, "smaller grow faster than larger" finding is a minimal, averaged way to account for what physically is more likely a near-constant slowing of the growth constant, k_j, with size of the discrete particles, j (and if one ignores for the moment the formation of magic-number size clusters, vide infra).
- The general "smaller grow more quickly than larger" finding is fully supported by this identical conclusion in an important 2019 report from Karim and his group at Virginia Tech,[55] in turn arguing for the greater generality of this paradigm-shifting insight. The strong evidence in the Karim-group Pd nanoparticle system for ligand-capping[54,55] as important in achieving these size-dependent growth rates is noteworthy and implies that ligand-capping step is likely applicable to the present Ir system and probably most other ligand-containing nanoparticle systems. Consistent with this, we have recently measured a rate decrease in the autocatalytic surface-growth k_2 rate constant with increasing [POM^{9-}], prima facie evidence for ligand capping in the system presented herein. Those findings are the subject of a separate paper.[85]
- The above support for ligand-capping effects on the growth rate constant so noted, remaining to be better understood are the finer details of ligand and other effects that can slow the growth rate with increasing particle size. In the present example, these potentially include the following effects: (i) that the POM^{9-} effective concentration compared to the Ir surface atoms goes from 1:1 in the $\{(1,5\text{-COD})Ir^{I}\cdot POM\}^{8-}$ precursor to ca. 9:1, for example, in the formation of POM^{9-} ligated $Ir(0)_{\sim 730}$ nanoparticles (i.e., and given that only ∼11% of the ∼730 Ir atoms are on the surface of an $Ir(0)_{\sim 730}$ nanoparticle); (ii) that the $\Delta H_{vaporization}$ = 159 kcal/mol (=27 kcal/mol average Ir−Ir BDE in at least bulk metal) means that smaller clusters are more energetic and hence expected to be more reactive toward growth than the larger ones; (iii) that smaller clusters likely have more Ir−H (per Ir) that we have postulated is more reactive in growth[23] (an excellent example of a reactive metal-hydride is the X-ray crystallography characterized $Ir_4H_4(1,5\text{-COD})_4$ cluster[86,87] which, when placed under H_2, is immediately reduced to bulk $Ir(0)_n$ in the absence of stabilizing ligands); and (iv) that smaller clusters have a higher number of low-metal coordination (e.g., kink or step) type sites that are often more reactive in catalysis[1,2] and, hence, are presumably more reactive in particle growth as well. Such particle-size dependent catalytic reactions are well known as "structure sensitive" catalytic reactions.[1,2]
- An important take-home message is that additional, where possible direct and multiple, simultaneous ways to monitor nucleation[88]—especially while detecting the smallest, sub-nanometer particles—will be critical en route to a better understanding of nucleation across nature.[6,18−26,52−56,88] Our own efforts are proceeding in two directions at present: (i) a $\{[(1,5\text{-COD})Ir\cdot HPO_4]_2\}^{2-}$ precursor system[89,90] exhibiting bimolecular nulceation[24] and where a combination of SAXS, XAFS, GLC, UV−visible, ^{1}H NMR, the CHCRR, TEM versus time PSDs, plus ME-PBM are currently being explored. Which methods give the most reliable rate constants, for example? Ideally, synthetic boundary crystallization ultracentrifugation employing a multiwavelength detector would be added to this list given its ability to detect the formation of M = metal $M_{1-3}^{0/n+}$ as well as $M_{\sim 13}$, $M_{\sim 55}$ and other magic-number[91] sized clusters.[92] Also under investigation by an array of physical methods, and in collaboration with Karim and his group, is (ii) a study of a promising $Ir^{I}(1,5\text{-COD})^{+}/POct_3$ precursors system, which permits isolation of novel, weakly ligated $Ir(0)_n\cdot(POct_3)_{0.2n}$ particles.[93]
- A valuable outgrowth of our long-term research of particle nucleation, growth, and agglomeration is that 19 classes of mechanisms and at least 48 distinct, reasonable mechanisms result from the pseudo-elementary steps in Scheme 1, plus the new three-step mechanism, all in combination with the A·L ⇌ A + L prior equilibrium,[23,54,55] plus the critical ligand-capping, pseudo-elementary step-based, B + L ⇌ B·L equilibrium[54] (i.e., and when one writes out all the possible different mechanisms in detail). Those mechanisms now can (and should) be tried in ME-PBModels to account for one's PSD and other data. This is a sizable advance when considering that, prior to 1997,[6] there were *zero* disproof-based, minimal mechanisms for particle formation. The availability of this broad range of ME-PBModels to try on one's particle formation data will hopefully reduce reports that either claim they have invented a new particle formation mechanism, when they have not,[94] as well as reduce reports that have failed to use any actual mechanism and, instead, employ empirical fitting functions—and then, unadvisedly, try unsuccessfully to reach physically meaningful conclusions from those empirical parameters.[95] Only if one of the ≥48 ME-PBMs will not account for your data, do you then have initial evidence for a new, pseudo-elementary-step based, particle formation mechanism.
- Last, it is worth emphasizing the significant difference between fitting PSDs, the loss of precursor A, and other kinetics data by ME-PBM as done herein in a disproof-based way that minimizes the number of adjustable parameters versus PBM studies yielding just simulations based on assumed mechanisms with a non-minimal number of adjustable parameters trying to match experimental data more or less "by eye". These are rather different topics with rather different physical outcomes and reliability, in our opinion.

Before closing, it is important to tie the present work into some other, noteworthy, relevant broader literature not yet mentioned herein. First, a paper elsewhere provides analytical formulas for all of the key points in sigmoidal nucleation-and-

https://dx.doi.org/10.1021/acs.jpcc.9b11239
J. Phys. Chem. C 2020, 124, 4852−4880

growth curves fit by the two-step mechanism (induction period; maximum slope; inflection point) in terms of k_1, k_2, and the starting precursor concentration A_o.[96] Second, full analytical solutions for the average size and polydispersity have recently appeared for the FW two-step mechanism for the case of bimolecular nucleation.[97] Third, a "Mathematical Model for Crystal Growth by Aggregation of Precursor Metastable Nanoparticles" has appeared[98] that, in their assumed mechanism I, provides an interesting comparison to the new three-step mechanism herein. That noteworthy paper hints at the greater generality of the ME-PBM approach developed herein and the resultant new three-step mechanism. A follow-up paper from those authors in 2006 also merits mention.[99] Fourth and finally, polymer chemists have addressed polymer product distribution problems that are different from the PSD problem addressed herein but still of considerable interest and hence recommended reading.[100−102]

Last, in a rather amazing case of "there is nothing new under the sun", while recently searching older literature related to our review of LaMer's 1950 model of particle formation,[5] we came across a quote in a little cited 1951 paper from LaMer's student Reiss.[103] Reiss was addressing the question that he obviously found perplexing regarding the LaMer model of "...why the 'growth by diffusion' should produce such uniform dispersions?". Reiss went on prophetically to note that "What is needed is some demonstration of the existence of a natural growth-regulating mechanism... This mechanism should permit nature to 'apply the brakes', so to speak, to retard the growth of larger particles while hastening the development of smaller ones." Remarkably, it has taken 69 years to uncover the evidence provided herein for, as well as the details of, just such a mechanism, the new three-step mechanism enabled with alternative termolecular nucleation.

7. CAVEATS AND A LOOK TO THE FUTURE

The above accomplishments, resultant insights, and broader literature so noted, much remains to be done in ME-PBM and related efforts. Specifically, (i) it remains to be experimentally tested whether the new three-step mechanism herein, or the FW two-step mechanism plus 2 ligand binding equilibria[54,55] added to it (or perhaps some hybrid of those two minimum mechanisms) is an overall more general or otherwise better description of particle formation across a broader range of systems when ligands are present. At least some of the needed studies are a focus of collaborative efforts in progress with Karim and his research group, with an emphasis on in situ, time-dependent SAXS data, other complimentary monitoring methods, plus ME-PBM. Additionally, it is important to (ii) obtain and understand the necessary component(s) the growth kernel that are required to produce very narrow, approaching monodisperse PSDs (as well as magic-number sized clusters). Mathematically and post implementation of the experimental nucleation mechanism, the mechanisms tested above are just different interpretations of the growth kernel. In the cases of the two- and three-step mechanisms, those with only monomer growth, the kernel is a function $f(n)$: $\mathbb{N} \rightarrow \mathbb{R}$ (i.e., a function from the natural numbers to the real numbers). In the case of the four-step, or any other mechanism including agglomeration, the kernel is $f(n, m)$: $\mathbb{N}^2 \rightarrow \mathbb{R}$, that is, it takes two natural numbers, one for each of the sizes agglomerating together, and yields a real number. The next goal here is to determine the mathematical requirements on these functions (the growth kernel) which guarantee near monodispersity. Ideally, this will then guide future experiments and methods to produce PSDs that are as close as possible to being monodispersed. The study of the necessary conditions can be done using a variable two-step mechanism, nearly identical to the FW two-step mechanism (eq 4), but where the rate *constant* k_2 for monomer growth is replaced by a size-dependent *function* $k_2(j)$. Furthermore, (ii) none of the above mechanisms and their ME-PBModels, nor anything in the literature, is able to explain kinetically and mechanistically why even our very first attempts at making $Ir(0)_n$ (as well as other) transition-metal nanoparticle syntheses back in the early 1990s yielded distributions that tend to center around full-shell, so-called magic-number sizes[40,41] (13, 55, 147, 309, 561, 923, and so on).[91] A question of interest here is whether or not our small versus large cutoff parameter, M, has any connection or correlation to magic-number clusters? Hence, understanding the formation of magic-number nanoparticles remains to be accomplished, something that would seem to demand that the growth rate constant and growth kernel as a function of size, $k_2(j)$, is *not* just a smoothly decreasing function.

Furthermore, (iv) one can now approach rationally the long-sought goal of upfront, mechanism-based-control of particle size and size-distribution in, for example, chemical catalysts. Important here is (v) that the concept of ME-PBM, and the ≥48 possible distinct ME-PBModels, promise to have much broader applicability across nature than just transition-metal nanoparticles such as $Ir(0)_n$ and $Pd(0)_m$. Required readings for anyone employing the two-step, three-step, or any of the other, deliberately minimalistic, pseudo-elementary-step mechanisms back in Scheme 1 are the published caveats and weaknesses of those mechanisms[4,22,23,81]—all of which derive from the overly simple nature of those deliberately minimalistic mechanisms.

Last, exciting is the potential broader extension of mechanism-enabled PBM to other "countable entities",[8] given that the powerful PBM formalism extends to systems in nature as varied as "the size and age distribution of fish in a lake, spatial distribution of cars on a freeway, activity and area distribution of particles in a catalysis bed, molecular distribution of polymer in a reactor, and size distribution of droplets in an emulsion",[8] among many, many other countable entities that form as distributions across nature. In short, the working hypotheses going forward, and demanding further testing across a broad range of countable entities in nature, is that the concept of ME-PBM promises to be much more generally applicable. Challenges that are apparent in fulfilling that promise include (i) determining the experimentally based nucleation mechanism for the system at hand and then (ii) implementing the PSD curve-fitting employed herein, tasks that become computationally intensive and hence more challenging for large particles (for which the full ODE approach may not be feasible), especially in systems where agglomeration is extensive. Our own efforts include trying to extend the full ODE approach to large, agglomerating systems. (iii) Being critically aware of the limitations of ME-PBM[104,105] promises to also be important in future efforts at ME-PBM.

■ ASSOCIATED CONTENT

Supporting Information

The Supporting Information is available free of charge at https://pubs.acs.org/doi/10.1021/acs.jpcc.9b11239.

Alternative attempted fits to diameter versus number of atoms; derivations: derivation of PBE; ODEs not

https://dx.doi.org/10.1021/acs.jpcc.9b11239
J. Phys. Chem. C 2020, 124, 4852−4880

presented in the main text for any of the six ME-PBMs in the main text: new three-step, ME-PBE; other ME-PBEquations examined en route to the six ME-PBEs given in the main text: lower order nucleation, two-step mechanism, simple first-order nucleation two-step mechanism, simulations and curve-fitting, second-order nucleation two-step mechanism, simulations and curve-fitting, fourth-order nucleation, two-step mechanism, simulations and curve-fitting, classic three-step mechanism in Scheme 3 of the main text, second four-step mechanism, and five-step, full agglomeration mechanism; experimental section: cyclohexene hydrogenation catalytic reporter reaction (CHCRR) kinetics, PSD data, measurement of K_{Diss} and k_{1alt}, and population balance modeling with PSD and CHCRR curve-fitting: resurrecting Smoluchowski's classic 1918 full ODE approach to the PBM (PDF)

AUTHOR INFORMATION

Corresponding Authors

Patrick D. Shipman − *Department of Mathematics, Colorado State University, Fort Collins, Colorado 80523-1874, United States;* orcid.org/0000-0003-4741-9370; Email: shipman@math.colostate.edu

Richard G. Finke − *Department of Chemistry, Colorado State University, Fort Collins, Colorado 80523, United States;* orcid.org/0000-0002-3668-7903; Email: Richard.Finke@colostate.edu

Authors

Derek R. Handwerk − *Department of Mathematics, Colorado State University, Fort Collins, Colorado 80523-1874, United States;* orcid.org/0000-0003-4614-9954

Christopher B. Whitehead − *Department of Chemistry, Colorado State University, Fort Collins, Colorado 80523, United States*

Saim Özkar − *Department of Chemistry, Middle East Technical University, 06800 Ankara, Turkey;* orcid.org/0000-0002-6302-1429

Complete contact information is available at: https://pubs.acs.org/10.1021/acs.jpcc.9b11239

Notes

The authors declare no competing financial interest.

ACKNOWLEDGMENTS

Professor A. Karim and his group at Virginia Tech are thanked for their input and helpful discussions, especially for sharing their own PBM efforts and important conclusions cited and referenced in the text based on their Pd/$POct_3$ nanoparticle system and studies.[54,55] Professor Phil Schneider of Murdoch University is thanked for valuable discussions on population balance modeling and the classic MoM approach. Also greatly appreciated are discussions with Professor Robert Waymouth at Stanford University regarding PBMs of PSDs in polymer chemistry.[102] We thank Pat Washecka-Jones for finding the small error in one line of our original code, as described in Section 2. This work was supported at Colorado State University by the U.S. Department of Energy (DOE), Office of Science, Office of Basic Energy Sciences, Division of Chemical Sciences, Geosciences & Biosciences, Catalysis Science program, via DOE grant SE-FG402-02ER15453, as well as the National Science Foundation Division of Mathematical Sciences, via NSF grant DMS-1814941.

GLOSSARY OF TERMS, VARIABLES, AND FUNCTIONS

CHCRR	cyclohexene catalytic reporter reaction
CNT	classical nucleation theory
ME-PBM	mechanism-enabled population balance modeling
MoM	method of moments
ODE	original differential equation
PB	population-balance
PBE	population balance equation
PBM	population balance modeling
PSD	particle size-distribution
A_{solv}	iridium solvate complex = $[(1,5\text{-COD})Ir^{I}(solv)_2]^+$
POM	**poly**o**xom**etalate ($P_2W_{15}Nb_3O_{62}^{9-}$)
S	solvent (solv)
V	volume
t	time
d	diameter
a	concentration of precursor monomers (mol/L)
n_j	concentration of particles of size j
m_j	$=j \times n_j$
b_j	concentration of binding sites on a particle of size j
k_i	rate constant
l	particle of size > M
M	cutoff size between "small" and "large" particles, B and C, respectively
$\hat{r}(j)$	growth kernel
$n(V,t)$	number of particles in the volume at time, t
$G(V,t)$	growth rate (volume/time)
$B(V,t)$	birth function (number/time)
$D(V,t)$	death function (number/time)

REFERENCES

(1) Che, M.; Bennett, C. O. The influence of particle size on the catalytic properties of supported metals. *Adv. Catal.* **1989**, *36*, 55−172.

(2) van Hardeveld, R.; Hartog, F. Influence of metal particle size on nickel-on-aerosol catalysts on surface site distribution, catalytic activity, and selectivity. *Adv. Catal.* **1972**, *22*, 75−113.

(3) Aiken, J. D., III; Lin, Y.; Finke, R. G. A perspective on nanocluster catalysis: polyoxoanion and $(n\text{-}C_4H_9)_4N^+$ stabilized $Ir(0)_{\sim 300}$ nanocluster 'soluble heterogeneous catalysts'. *J. Mol. Catal. A: Chem.* **1996**, *114*, 29−51.

(4) Laxson, W. W.; Finke, R. G. Nucleation is second order: an apparent kinetically effective nucleus of two for $Ir(0)_n$ nanoparticle formation from $[(1,5\text{-COD})Ir^{I}\bullet P_2W_{15}Nb_3O_{62}]^{8-}$ plus hydrogen. *J. Am. Chem. Soc.* **2014**, *136*, 17601−17615. Please also see the references provided therein to CNT and other relevant literature.

(5) Whitehead, C. B.; Özkar, S.; Finke, R. G. LaMer's 1950 model for particle formation of instantaneous nucleation and diffusion-controlled growth: a historical look at the model's origins, assumptions, equations, and underlying sulfur sol formation kinetics data. *Chem. Mater.* **2019**, *31*, 7116−7132.

(6) Watzky, M. A.; Finke, R. G. Transition metal nanocluster formation kinetic and mechanistic studies. A new mechanism when hydrogen is the reductant: slow, continuous nucleation and fast autocatalytic surface growth. *J. Am. Chem. Soc.* **1997**, *119*, 10382−10400.

(7) Handwerk, D. R.; Shipman, P. D.; Whitehead, C. B.; Özkar, S.; Finke, R. G. Mechanism-enabled population balance modeling of particle formation en route to particle average size and size distribution understanding and control. *J. Am. Chem. Soc.* **2019**, *141*, 15827−15839.

(8) Randolph, A. D. A population balance for countable entities. *Can. J. Chem. Eng.* **1964**, *42*, 280−281.

(9) Hulburt, H. M.; Katz, S. Some problems in particle technology. A statistical mechanical formulation. *Chem. Eng. Sci.* **1964**, *19*, 555−574.
(10) Randolph, A. D.; Larson, M. A. The Population Balance. *Theory of Particulate Processes. Analysis and Techniques of Continuous Crystallization*; Academic Press: New York and London, 1971; p 46 for MaCabe's law, which states that the growth rate is independent of diameter (length) of the particles.
(11) Ramkrishna, D. The status of population balances. *Rev. Chem. Eng.* **1985**, *3*, 49−95. see p 88 for the cited quote
(12) Ramkrishna, D. Population Balances. *Theory and Application to Particulate Systems in Engineering*; Academic Press: New York, 2000.
(13) Ramkrishna, D.; Mahoney, A. W. Population balance modeling. Promise for the future. *Chem. Eng. Sci.* **2002**, *57*, 595−606.
(14) Vetter, T.; Iggland, M.; Ochsenbein, D. R.; Hänseler, F. S.; Mazzotti, M. Modeling nucleation, growth, and ostwald ripening in crystallization processes: A comparison between population balance and kinetic rate equation. *Cryst. Growth Des.* **2013**, *13*, 4890−4905.
(15) Farhadi, F.; Babaheidary, M. B. Mechanism and estimation of $Al(OH)_3$ crystal growth. *J. Cryst. Growth* **2002**, *234*, 721−730.
(16) Chamberlin, T. C. Studies for students. The method of multiple working hypotheses. *J. Geol.* **1897**, *5*, 837−848.
(17) Platt, J. R. Strong Inference: Certain systematic methods of scientific thinking may produce much more rapid progress than others. *Science* **1964**, *146*, 347−353.
(18) Hornstein, B. J.; Finke, R. G. Transition-metal nanocluster kinetic and mechanistic studies emphasizing nanocluster agglomeration: demonstration of a kinetic method that allows monitoring of all three phases of nanocluster formation and aging. *Chem. Mater.* **2004**, *16*, 139−150. (See also the addition/correction: *Chem. Mater.* **2004**, *16*, 3972.)
(19) Besson, C.; Finney, E. E.; Finke, R. G. A mechanism for transition-metal nanoparticle self-assembly. *J. Am. Chem. Soc.* **2005**, *127*, 8179−8184.
(20) Besson, C.; Finney, E. E.; Finke, R. G. Nanocluster nucleation, growth and then agglomeration kinetic and mechanistic studies: a more general, four-step mechanism involving double autocatalysis. *Chem. Mater.* **2005**, *17*, 4925−4938.
(21) Finney, E. E.; Finke, R. G. The four-step, double-autocatalytic mechanism for transition-metal nanocluster nucleation, growth and then agglomeration: metal, ligand, concentration, temperature, and solvent dependency studies. *Chem. Mater.* **2008**, *20*, 1956−1970.
(22) Kent, P. D.; Mondloch, J. E.; Finke, R. G. A four-step mechanism for the formation of supported-nanoparticle heterogeneous catalysts in contact with solution: the conversion of Ir(1,5-COD)Cl/γ-Al_2O_3 to $Ir(0)_{\sim 170}$/γ-Al_2O_3. *J. Am. Chem. Soc.* **2014**, *136*, 1930−1941.
(23) Özkar, S.; Finke, R. G. Nanoparticle nucleation is termolecular in metal and involves hydrogen: evidence for a kinetically effective nucleus of three $\{Ir_3H_{2x}\bullet P_2W_{15}Nb_3O_{62}\}^{6-}$ in $Ir(0)_n$ nanoparticle formation from $[(1,5\text{-COD})Ir^{I}\bullet P_2W_{15}Nb_3O_{62}]^{8-}$ plus dihydrogen. *J. Am. Chem. Soc.* **2017**, *139*, 5444−5457. Please also see the references provided therein.
(24) Whitehead, C. B.; Finke, R. G. Nucleation kinetics and molecular mechanism in transition-metal nanoparticle formation: the intriguing, informative case of a bimetallic precursor, $\{[(1,5\text{-COD})Ir^{I}\bullet HPO_4]_2\}^{2-}$. *Chem. Mater.* **2019**, *31*, 2848−2862. Please also see the references provided therein.
(25) Finney, E. E.; Finke, R. G. Nanocluster nucleation and growth kinetic and mechanistic studies: a review emphasizing transition-metal nanoclusters. *J. Colloid Interface Sci.* **2008**, *317*, 351−374.
(26) Özkar, S.; Finke, R. G. Dust effects on nucleation kinetics and nanoparticle product size distributions: the illustrative case study of a prototype Ir(0)n transition-metal nanoparticle formation system. *Langmuir* **2017**, *33*, 6550−6562. See also the references in this paper to the history and prior key literature on the effects of dust on particle formation and nucleation kinetics.
(27) Hounslow, M. J.; Ryall, R. L.; Marshall, V. R. A discretized population balance for nucleation, growth, and aggregation. *AIChE J.* **1988**, *34*, 1821−1832.
(28) Parbhakar, K.; Jin, J.-M.; Dao, L. H. Kinetic analytic model for time-dependent growth of particles. *J. Colloid Interface Sci.* **1995**, *174*, 414−420.
(29) Van Hyning, D. L.; Klemperer, W. G.; Zukoski, C. F. Silver nanoparticle formation: predictions and verification of the aggregative growth model. *Langmuir* **2001**, *17*, 3128−3135.
(30) Dixit, N. M.; Zukoski, C. F. Nucleation rates and induction times during colloidal crystallization: links between models and experiments. *Phys. Rev. E: Stat., Nonlinear, Soft Matter Phys.* **2002**, *66*, 051602.
(31) Kulkarni, A. M.; Zukoski, C. F. Nanoparticle crystal nucleation: influence of solution conditions. *Langmuir* **2002**, *18*, 3090−3099.
(32) Ethayaraja, M.; Dutta, K.; Bandyopadhyaya, R. Mechanism of nanoparticle formation in self-assembled colloidal templates: population balance model and monte carlo simulation. *J. Phys. Chem. B* **2006**, *110*, 16471−16481.
(33) Somasundaran, P.; Runkana, V. Aggregation of colloids: recent developments of population balance modeling. *Highlights in Colloidal Science*; Platikanov, D., Exerowa, D., Eds.; Wiley-VCH Verlag, 2009.
(34) Woehl, T. J.; Park, C.; Evans, J. E.; Arslan, I.; Ristenpart, W. D.; Browning, N. D. Direct observation of aggregative nanoparticle growth: kinetic modeling of the size distribution and growth rate. *Nano Lett.* **2014**, *14*, 373−378.
(35) Taboadaserrano, P.; Chin, C.; Yiacoumi, S.; Tsouris, C. Modeling aggregation of colloidal particles. *Curr. Opin. Colloid Interface Sci.* **2005**, *10*, 123−132.
(36) Vanni, M. Approximate population balance equations for aggregation-breakage processes. *J. Colloid Interface Sci.* **2000**, *221*, 143−160.
(37) Somasundaran, P.; Runkana, V. Modeling flocculation of colloidal mineral suspensions using population balances. *Int. J. Miner. Process.* **2003**, *72*, 33−55.
(38) Thomas, D. N.; Judd, S. J.; Fawcett, N. Flocculation modelling: a review. *Water Res.* **1999**, *33*, 1579−1592.
(39) Galbraith, S. C.; Schneider, P. A. Modelling and simulation of inorganic precipitation with nucleation, crystal growth and aggregation: A new approach to an old method. *Chem. Eng. J.* **2014**, *240*, 124−132.
(40) Lin, Y.; Finke, R. G. Novel polyoxoanion and Bu_4N^+ stabilized, isolable, and redissolvable, 20-30 Å $Ir_{\sim 300\text{-}900}$ nanoclusters: the kinetically controlled synthesis, characterization, and mechanism of formation of organic solvent-soluble, reproducible size, and reproducible catalytic activity metal nanoclusters. *J. Am. Chem. Soc.* **1994**, *116*, 8335−8353.
(41) Lin, Y.; Finke, R. G. A more general approach to distinguishing "homogeneous" from "heterogeneous" catalysis: discovery of polyoxoanion- and Bu_4N^+-stabilized, isolable and redissolvable, high reactivity $Ir_{\sim 190-450}$ nanocluster catalysts. *Inorg. Chem.* **1994**, *33*, 4891−4910.
(42) Volmer, M.; Weber, A. Z. Keimbildung in übersättigten Gebilden. *Z. Phys. Chem.* **1926**, *119*, 277.
(43) Tohmfor, G.; Volmer, M. Die keimbildung unter dem einfluß elektrischer ladungen. *Ann. Phys.* **1938**, *425*, 109−131.
(44) Volmer, M. *Kinetik der Phasenbildung*; Verlag von Theodor Steinkopff: Leipzig, 1939.
(45) Becker, R.; Döring, W. Kinetische behandlung der keimbildung in übersaettigten Dampfen. *Ann. Phys.* **1935**, *416*, 719−752.
(46) Kashchiev, D. *Nucleation: Basic Theory with Applications*; Butterworth Heinemann: Oxford, U.K., 2000.
(47) Oxtoby, D. W. Homogeneous nucleation: theory and experiment. *J. Phys.: Condens. Matter* **1992**, *4*, 7627−7650.
(48) Zhang, T. H.; Liu, X. Y. Nucleation: what happens at the initial stage? *Angew. Chem., Int. Ed.* **2009**, *48*, 1308−1312.
(49) Erdemir, D.; Lee, A. Y.; Myerson, A. S. Nucleation for crystals from solution: classical and two-step models. *Acc. Chem. Res.* **2009**, *42*, 621−629. Note the "Two-Step Model" referred to in this work and associated literature, involving an amorphous, pre-nucleation, dense phase and/or clusters, is distinct from and should not be confused with the FW 2-step mechanism[6] of continuous nucleation and autocatalytic surface growth.

https://dx.doi.org/10.1021/acs.jpcc.9b11239
J. Phys. Chem. C 2020, 124, 4852−4880

(50) *Nucleation—a Transition State to the Directed Assembly of Materials*; Faraday Discussions; Royal Society Of Chemistry: U.K., 2015; Vol. *179*, pp 9−154.
(51) Zhang, R.; Khalizov, A.; Wang, L.; Hu, M.; Xu, W. Nucleation and growth of nanoparticles in the atmosphere. *Chem. Rev.* **2012**, *112*, 1957−2011. The "strongly associated" systems in this review correspond in a general way to what we denote as "strongly bonded" systems in the present research.
(52) Perala, S. R. K.; Kumar, S. On the two-step mechanism for synthesis of transition-metal nanoparticles. *Langmuir* **2014**, *30*, 12703−12711.
(53) Field, R. J.; Noyes, R. M. Oscillations in chemical systems. 18. Mechanisms of chemical oscillators: conceptual bases. *Acc. Chem. Res.* **1977**, *10*, 214−221. Please also see the references provided therein. As we first noted in footnote 31 elsewhere,[4] "The concept of pseudoelementary steps was introduced in the 1970s by Noyes, who developed this concept using kinetic studies of complex oscillating reactions. By pseudo-elementary we mean collections of one or more slow steps, plus any number of faster steps, that when added together yield a balanced reaction that can be uses as effectively elementary (i.e., as pseudo-elementary) for the purposes of kinetic treatments in the same way that truly elementary steps are used as the basic building blocks of reliable reaction mechanisms. That said, the reaction order of a pseudo-elementary step cannot be directly used to imply the molecularity of that (composite) step as is the case with a true elementary step".
(54) Mozaffari, S.; Li, W.; Thompson, C.; Ivanov, S.; Seifert, S.; Lee, B.; Kovarik, L.; Karim, A. M. Colloidal nanoparticle size control: experimental and kinetic modeling investigation of the ligand-metal binding role in controlling the nucleation and growth kinetics. *Nanoscale* **2017**, *9*, 13772−13785.
(55) Mozaffari, S.; Li, W.; Dixit, M.; Seifert, S.; Lee, B.; Kovarik, L.; Mpourmpakis, G.; Karim, A. M. The role of nanoparticle size and ligand coverage in size focusing of colloidal metal nanoparticles. *Nanoscale Adv.* **2019**, *1*, 4052−4066.
(56) Smith, S. E.; Sasaki, J. M.; Bergman, R. G.; Mondloch, J. E.; Finke, R. G. Platinum-catalyzed phenyl and methyl group transfer from tin to iridium: evidence for an autocatalytic reaction pathway with an unusual preference for methyl transfer. *J. Am. Chem. Soc.* **2008**, *130*, 1839−1841. See the accompanying Supporting Information for the details of how the true elementary steps were deduced, and how they add up to the pseudo-elementary steps that proved necessary, and were used first, to uncover the underlying, elementary-step mechanism—one supported in this case by direct monitoring of all observable species in the catalytic cycle.
(57) Falola, A.; Borissova, A.; Wang, X. Z. Extended method of moment for general population balance models including size dependent growth rate, aggregation and breakage kernels. *Comput. Chem. Eng.* **2013**, *56*, 1−11.
(58) Sporleder, F.; Borka, Z.; Solsvik, J. On the population balance equation. *Rev. Chem. Eng.* **2012**, *28*, 149−169.
(59) Kumar, S.; Ramkrishna, D. On the solution of population balance equations by discretization—I. A fixed pivot technique. *Chem. Eng. Sci.* **1996**, *51*, 1311−1332.
(60) Nguyen, T. T.; Laurent, F.; Fox, R. O.; Massot, M. Solution of population balance equations in applications with fine particles: Mathematical modeling and numerical schemes. *J. Comput. Phys.* **2016**, *325*, 129−156.
(61) Liao, Y.; Oertel, R.; Kriebitzsch, S.; Schlegel, F.; Lucas, D. A discrete population balance equation for binary breakage. *Int. J. Numer. Methods Fluids* **2018**, *87*, 202−215.
(62) Rigopoulos, S. Population balance modelling of polydispersed particles in reactive flows. *Prog. Energy Combust. Sci.* **2010**, *36*, 412−443.
(63) Smoluchowski, M. V. Versuch einer mathematischen theorie der koagulationskinetik kolloider lösungen. *Z. Phys. Chem.* **1918**, *92*, 129−168. A December 1, 2019 Web of Science search of this paper and refining the 228 hits by "population balance modeling" yielded only 3 papers.
(64) Chandrasekhar, S. Stochastic problems in physics and astronomy. *Rev. Mod. Phys.* **1943**, *15*, 1−89. This review provides a summary in English of Smoluchowski's 1918 paper.
(65) Hoffmann, R.; Minkin, V. I.; Carpenter, B. K. Ockham's razor and chemistry. *Bull. Soc. Chim. Fr.* **1996**, *133*, 117−130.
(66) Schmidt, A. F.; Smirnov, V. V. Concept of "magic" number clusters as a new approach to the interpretation of unusual kinetics of the Heck reaction with aryl bromides. *Top. Catal.* **2005**, *32*, 71−75. Note that the surface-atom approximation given by Schmidt and Smirnov has more surface atoms than total atoms for particles smaller than 34. Using this approximation verbatim makes the function r not directly correspond to a percentage of total atoms that are bindable, at least for small sizes. This has the effect of making smaller sized atoms more reactive than a strictly surface area dependent growth model. The piecewise function $r = \begin{Bmatrix} 1, & j < 34 \\ s(j), & j \geq 34 \end{Bmatrix}$, where j is the particle size and $s(j)$ is the Schmidt and Smirnov approximation would be a modification that does not have this deficiency.
(67) Bayram, E.; Lu, J.; Aydin, C.; Browning, N. D.; Özkar, S.; Finney, E.; Gates, B. C.; Finke, R. G. Agglomerative sintering of an atomically dispersed Ir_1/zeolite Y catalyst: compelling evidence against ostwald ripening but for bimolecular and autocatalytic agglomeration catalyst sintering steps. *ACS Catal.* **2015**, *5*, 3514−3527.
(68) Pawluk, T.; Hirata, Y.; Wang, L. Studies of iridium nanoparticles using density functional theory calculations. *J. Phys. Chem. B* **2005**, *109*, 20817−20823. These DFT calculations predict that (naked; unligated) Ir particles prefer a rigid cubic structure until a 48-atom particle (5.91 eV per Ir atom binding energy) is reached, at which point a transition to face-centered cubic occurs. This 48-atom (about 1.1 nm diameter) limit hinders coalescence of at least naked, smaller nanoparticles because energetically unfavorable surface rearrangements would be required—again, with the caveat here that these calculations refer strictly to only naked, unligated iridium nanoparticles.
(69) LaMer, V. K.; Dinegar, R. H. Theory, production and mechanism of formation of monodispersed hydrosols. *J. Am. Chem. Soc.* **1950**, *72*, 4847−4854.
(70) As detailed in the Experimental section, an estimate of $K_{Diss,\ apparent} = K_{Diss}[solvent]^2 = (6.4 \pm 1.4) \times 10^{-5}$ M at 25 °C was measured by ^{31}P NMR, originally in propylene carbonate[23] (where $[Solvent]^2 = (12.1\ M)^2$ for neat propylene carbonate). This in turn yields a $K_{Diss} \approx 5 \times 10^{-7}\ M^{-1}$ value that was used in the ME-PBM, along with $[solvent]^2 = (11.3\ M)^2$ for 2.5 mL acetone and 0.5 mL cyclohexene (i.e., and given that neat acetone is 13.6 M). Moreover, as an experimental check on this value and the above assumption, a K_{Diss}(acetone) of ∼5×10^{-7} M 25 °C was actually measured by ^{31}P NMR in acetone following the published methods.[23] (Note here that this corrects one word in footnote 47 of our first ME-PBM paper where it said "$(11.3\ M)^2$ for 2.5 mL propylene carbonate" but where it should have said "$(11.3\ M)^2$ for 2.5 mL *acetone*").
(71) It has not escaped our notice that, logically, this insight bears on the minimum mechanisms themselves in Scheme 3 that were used to enable the PBMs in the first place (and given that the CHCRR is a primary, albeit certainly not the only, source of kinetics and other evidence for those mechanisms). This caveat so noted, additional evidence for the minimum mechanisms in Scheme 1 is available including: the balanced reaction stoichiometries, the closer to direct monitoring of the loss of the precursor, A, by its cyclooctane reaction product by GLC or ^{1}H NMR, a critical control first done in the original 1997 paper[6] to show that the CHCRR method looked to be faithfully reproducing those kinetics in at least the first ca. one-third to one-half of the CHCRR curve, so far as could be determined as the time; the TEM-derived PSDs, and now and importantly the ME-PBM herein that strongly supports for example the alternative termolecular nucleation mechanism[23] discovered primarily using the CHCRR methodology. The basic features of the FW 2-step mechanism are also strongly if not overwhelmingly supported by its >560 citations to date that include use of the 2-step mechanism to fit sigmoidal nucleation and growth kinetics curves, obtained by pretty much all applicable physical methods, and for multiple systems across nature that exhibit sigmoidal kinetics.

https://dx.doi.org/10.1021/acs.jpcc.9b11239
J. Phys. Chem. C 2020, 124, 4852−4880

(72) Yin, C.-X.; Finke, R. G. Kinetic and mechanistic studies of vanadium-based, extended catalytic lifetime catechol dioxygenases. *J. Am. Chem. Soc.* **2005**, *127*, 13988−13996.
(73) Bayram, E.; Linehan, J. C.; Fulton, J. L.; Roberts, J. A. S.; Szymczak, N. K.; Smurthwaite, T. D.; Özkar, S.; Balasubramanian, M.; Finke, R. G. Is it homogeneous or heterogeneous catalysis derived from $[RhCp^*Cl_2]_2$? In operando XAFS, kinetic, and crucial kinetic poisoning evidence for subnanometer Rh4 cluster-based benzene hydrogenation catalysis. *J. Am. Chem. Soc.* **2011**, *133*, 18889−18902.
(74) Mondloch, J. E.; Wang, Q.; Frenkel, A. I.; Finke, R. G. Development plus kinetic and mechanistic studies of a prototype supported-nanoparticle heterogeneous catalyst formation system in contact with solution: Ir(1,5-COD)Cl/γ-Al_2O_3 and Its Reduction by H_2 to $Ir(0)_n$/γ-Al_2O_3. *J. Am. Chem. Soc.* **2010**, *132*, 9701−9714.
(75) Mondloch, J. E.; Finke, R. G. Supported-nanoparticle heterogeneous catalyst formation in contact with solution: kinetics and proposed mechanism for the conversion of Ir(1,5-COD)Cl/γ-Al_2O_3 to $Ir(0)_{\sim 900}$/γ-Al_2O_3. *J. Am. Chem. Soc.* **2011**, *133*, 7744−7756.
(76) Mondloch, J. E.; Bayram, E.; Finke, R. G. A review of the kinetics and mechanisms of formation of supported-nanoparticle heterogeneous catalysts. *J. Mol. Catal. A: Chem.* **2012**, *355*, 1−38.
(77) Morris, A. M.; Watzky, M. A.; Agar, J. N.; Finke, R. G. Fitting neurological protein aggregation kinetic data via a 2-step, minimal/"Ockham's razor" model: the Finke-Watzky mechanism of nucleation followed by autocatalytic surface growth. *Biochem* **2008**, *47*, 2413−2427.
(78) Watzky, M. A.; Morris, A. M.; Ross, E. D.; Finke, R. G. Fitting yeast and mammalian prion aggregation kinetic data with the Finke-Watzky two-step model of nucleation and autocatalytic growth. *Biochem* **2008**, *47*, 10790−10800.
(79) Morris, A. M.; Finke, R. G. α-Synuclein aggregation variable temperature and variable pH kinetic data: a re-analysis using the Finke-Watzky 2-step model of nucleation and autocatalytic growth. *Biophys. Chem.* **2009**, *140*, 9−15.
(80) Morris, A. M.; Watzky, M. A.; Finke, R. G. Protein aggregation kinetics, mechanism, and curve-fitting: A review of the literature. *Biochim. Biophys. Acta, Proteins Proteomics* **2009**, *1794*, 375−397.
(81) Finney, E. E.; Finke, R. G. Is there a minimal chemical mechanism underlying classical Avrami-Erofe'ev treatments of phase transformation kinetic data? *Chem. Mater.* **2009**, *21*, 4692−4705.
(82) Tong, F.; Hanson, M. P.; Bardeen, C. J. Analysis of reaction kinetics in the photomechanical molecular crystal 9-methylanthracene using an extended Finke-Watzky model. *Phys. Chem. Chem. Phys.* **2016**, *18*, 31936−31945.
(83) Avinash, M. B.; Sandeepa, K. V.; Govindaraju, T. Emergent behaviors in kinetically controlled dynamic self-assembly of synthetic molecular systems. *ACS Omega* **2016**, *1*, 378−387.
(84) Oladoja, N. A. A critical review of the applicability of Avrami fractional kinetic equation in adsorption-based water treatment studies. *Desalin. Water Treat.* **2015**, *57*, 15813−15825.
(85) Özkar, S.; Finke, R. G. Nanoparticle formation kinetics and mechanistic studies important to mechanism-based particle-size control: evidence for ligand-based slowing of the autocatalytic surface growth step plus postulated mechanisms. *J. Phys. Chem. C* **2019**, *123*, 14047−14057.
(86) Yih, K.-H.; Hamdemir, I. K.; Mondloch, J. E.; Bayram, E.; Özkar, S.; Vasić, R.; Frenkel, A. I.; Anderson, O. P.; Finke, R. G. Synthesis and characterization of $[(1,5\text{-Cyclooctadiene})Ir(\mu\text{-H})]_4$: a tetrametallic Ir4H4-core coordinatively unsaturated cluster. *Inorg. Chem.* **2012**, *51*, 3186−3193.
(87) Laxson, W. W.; Özkar, S.; Folkman, S.; Finke, R. G. The story of a mechanism-based solution to an irreproducible synthesis resulting in an unexpected closed-system requirement for the $LiBEt_3H$-based reduction: the case of the novel subnanometer cluster, $[Ir(1,5\text{-COD})(\mu\text{-H})]_4$, and the resulting improved, independently repeatable, reliable synthesis. *Inorg. Chim. Acta* **2015**, *432*, 250−257.
(88) Georgiev, P.; Bojinova, A.; Kostova, B.; Momekova, D.; Bjornholm, T.; Balashev, K. Implementing atomic force microscopy (AFM) for studying kinetics of gold nanoparticle's growth. *Colloids Surf., A* **2013**, *434*, 154−163. This valuable paper examines: AFM, STEM, TEM, DLE, and UV-vis (the latter with proper accounting for the plasmon resonance as a function of the particle size) and its effect on the k_1 and k_2 rate constants from fits to the FW 2-step model. The k_1 and k_2 values from the various methods differ by respective factors of 10−38 for k_1 vs just ∼2 for k_2, showing that determining precise nucleation, k_1, rate constants is challenging and often problematic
(89) Özkar, S.; Finke, R. G. Transition-metal nanocluster stabilization fundamental studies: hydrogen phosphate as a simple, effective, readily available, robust, and previously unappreciated stabilizer for well-formed, isolable, and redissolvable Ir(0) and other transition-metal nanoclusters. *Langmuir* **2003**, *19*, 6247−6260.
(90) Özkar, S.; Finke, R. G. The hydrogenphosphate complex of (1,5-cyclooctadiene)Iridium(I), $\{[Bu_4N][(1,5\text{-COD})Ir{\bullet}HPO_4]\}_n$: synthesis, spectroscopic characterization, and ES-MS of a new, preferred precursor to HPO_4^{2-} and Bu_4N^+ stabilized $Ir(0)_n$ nanoclusters. *J. Organomet. Chem.* **2004**, *689*, 493−501.
(91) Teo, B. K.; Sloane, N. J. A. Magic numbers in polygonal and polyhedral clusters. *Inorg. Chem.* **1985**, *24*, 4545−4558.
(92) Völkle, C. M.; Gebauer, D.; Cölfen, H. High-resolution insights into the early stages of silver nucleation and growth. *Faraday Discuss.* **2015**, *179*, 59−77.
(93) Mondloch, J. E.; Özkar, S.; Finke, R. G. "Weakly ligated, labile ligand" nanoparticles: the case of $Ir(0)_n{\bullet}(H^+Cl^-)_m$. *ACS Omega* **2018**, *3*, 14538−14550.
(94) Watzky, M. A.; Finke, R. G. Gold nanoparticle formation kinetics and mechanism: a critical analysis of the putative "Redox Crystallization" mechanism. *ACS Omega* **2018**, *3*, 1555−1563.
(95) Özkar, S.; Finke, R. G. Silver nanoparticles synthesized by microwave heating: a kinetic and mechanistic re-analysis and re-interpretation. *J. Phys. Chem. C* **2017**, *121*, 27643−27654.
(96) Bentea, L.; Watzky, M. A.; Finke, R. G. Sigmoidal nucleation and growth curves across nature fit by the Finke-Watzky model of slow continuous nucleation and autocatalytic growth: explicit formulas for the lag and growth times plus other key insights. *J. Phys. Chem. C* **2017**, *121*, 5302−5312.
(97) Szabó, R.; Lente, G. Full analytical solution of a nucleation-growth type kinetic model of nanoparticle formation. *J. Math. Chem.* **2019**, *57*, 616−631.
(98) Drews, T. O.; Katsoulakis, M. A.; Tsapatsis, M. Mathematical model for crystal growth by aggregation of precursor metastable nanoparticles. *J. Phys. Chem. B* **2005**, *109*, 23879−23887. This 2005 paper is a noteworthy contribution, especially for its 14-year earlier time, perhaps being the best prior attempt at what we denote herein as ME-PBM. Note that the authors preferred their more complex, 4-step Mechanism II (that has a typo in the second step; it should be $B \rightarrow C_1$, and not the repetitive $B + C_i \rightarrow C_{i+1}$). The importance of this paper 2005 paper so noted, key advances reported in our present, 2019 paper critical to true ME-PBM include: the input of disproof-based, experimentally known nucleation and growth mechanism; quantitative fitting of the PSD; and the key finding of a particle-size-dependent growth as documented in the present, 2019 paper.
(99) Davis, T. M.; Drews, T. O.; Ramanan, H.; He, C.; Dong, J.; Schnablegger, H.; Katsoulakis, M. A.; Kokkoli, E.; McCormick, A. V.; Penn, R. L.; et al. Mechanistic principles of nanoparticle evolution to zeolite crystals. *Nat. Mater.* **2006**, *5*, 400−408. This valuable paper reports a prolonged nucleation stage for the zeolite crystal growth with gradual loss of precursor. The nucleation mechanism is not known (is assumed to be first order and reversible), nor is the primary growth mechanism known (a second step of reversible bimolecular agglomeration of B + B to C is assumed), so that while quite interesting, this work does not qualify as ME-PBM by the definition given in the present, 2019 ME-PBM paper. Additionally, the authors assume a constant growth rate for all particle sizes, another critical difference from the 3-step in the present work. Relevant here is that a 2-step mechanism with its two irreversible steps and two (k_1 and k_2) rate-constant parameters has been shown to fit the Figure 6 zeolite yield vs time data better (see Figure S5 of the Supporting Information of a 2009 paper[81]) than does the 4 parameter model employed in the 2006

https://dx.doi.org/10.1021/acs.jpcc.9b11239
J. Phys. Chem. C 2020, 124, 4852−4880

paper.[99] Nevertheless, the most important point is that both this 2006[99] and the prior 2005 study[98] are valuable earlier studies on the edge of being ME-PBM.

(100) A close inspection reveals that the underlying mechanisms and hence accompanying ODEs of initiation and polymerization are not unexpectedly different than those for particle formation. The differences arise due to the monomer and initiator in polymerization reactions being supplied in known concentrations vs "monomer" or actually bimetallic[24] or termolecular[23] precursors being generated as part of nucleation, growth, and agglomeration in particle formation reactions. Another difference between polymerizations and particle formations is that in a polymerization there is typically just one site from which the polymer grows, while growth in a nanoparticle is possible across multiple surface sites and is surface-ligand dependent.[54] These differences so noted, the cited two excellent, relevant contributions from the polymer distributions literature are recommended reading.[101,102]

(101) Gold, L. Statistics of polymer molecular size distribution for an invariant number of propagating chains. *J. Chem. Phys.* **1958**, *28*, 91−99.

(102) Brown, H. A.; Xiong, S.; Medvedev, G. A.; Chang, Y. A.; Abu-Omar, M. M.; Caruthers, J. M.; Waymouth, R. M. Zwitterionic ring-opening polymerization: models for kinetics of cyclic poly(caprolactone) synthesis. *Macromolecules* **2014**, *47*, 2955−2963. Noteworthy in this paper are: (i) the similar approach of a disproof-based, minimalistic mechanism to start; (ii) the slow initiation, fast propagation polymerization system; (iii) the monomer addition steps in the mechanism; and (iv) the finding that such a system can lead to a relatively narrow size distribution—all features closely paralleling those in the present, nanoparticle ME-PBM study. Two major differences, however, are: (iv) the underlying mechanism is fundamentally different than any in the present nanoparticle study, and (v) a Monte Carlo, stochastic simulation had to be used due to the high polymer MWs and, hence, many monomer addition steps (vs the full ODE approach possible for our nanoparticle formation reaction and its order of magnitude fewer number of steps). Nevertheless, this excellent work is an example that fits our definition of ME-PBM, albeit now in polymer chemistry, something that expands the scope and impact of the concept of Mechanism-Enabled PBModeling. We thank Prof. Waymouth for stimulating discussion of the PBMs of polymer vs particle formation systems.

(103) Reiss, H. The growth of uniform colloidal dispersions. *J. Chem. Phys.* **1951**, *19*, 482−487.

(104) Repeating and expanding on those limitations as listed in our recent paper:[7] "Current limitations of ME-PBM and the full ODE approach that are apparent at present include the following: (i) the desire for more detailed, experimentally based mechanisms (i.e., beyond the deliberately minimum mechanisms in Scheme 3) as even better input into one's ME-PBM; (ii) the increasing computation time required for the full-ODE approach once the particles get larger and larger; and (iii) the much greater computational time required when agglomeration is part of the particle-formation process (and, hence, the difficulties to impossibility of implementing the full ODE approach where agglomeration is occurring, especially for larger final particle sizes)." To these limitations we can add cautions that are not about the ME-PBM itself, but about the data one needs to collect for optimal ME-PBM, issues explored in part in an upcoming paper:[105] (a) one wants to monitor the particle formation reaction by as many, and ideally as many direct, physical methods as possible; (b) one wants to be sure one has as a minimum a way to follow not just the PSD, but also the loss of precursor, A (and as done herein via the CHCRR, even if an indirect method); (c) one want to monitor the PSDs as a function of time, and then and of course know the precise times at which the PSDs where obtained (as is required in ME-PBM analysis of the kinetics); and (d) one wants of course to reduce the number of fit variables to the minimum possible by, for example, measuring independently and then inputting any and all constants possible (such as done with K_{Diss} and k_{1alt} in the present work)—that is, one wants to fully enable with as much experimental information as possible the ME-PBM.

(105) Handwerk, D. R.; Shipman, P. D.; Özkar, S.; Finke, R. G. Dust effects on $Ir(0)_n$ nanoparticle formation nucleation and growth kinetics and particle-size Distributions: analysis by and insights from mechanism-enabled population balance modeling. *Langmuir* **2020**, DOI: 10.1021/acs.langmuir.9b03193. This paper addresses in greater detail the steps and issues involved in multi-parameter fitting using ME-PBM analysis of PSDs and other kinetics data.

https://dx.doi.org/10.1021/acs.jpcc.9b11239
J. Phys. Chem. C 2020, 124, 4852−4880